ÉCOLE POLYTECHNIQUE FÉDÉRALE DE LAUSANNE

MATHICSE

Mathematics Institute of Computational Science and Engineering

School of Basic Sciences - Section of Mathematics

MATHICSE Technical Report

Nr. 2.2012

January 2012

Time accurate partitioned algorithms for the solution of fluid-structure interaction problems in haemodynamics

Fabio Nobile, Matteo Pozzoli, Christian Vergara

http://mathicse.epfl.ch

Phone: +41 21 69 37648

Address:
EPFL - SB - MATHICSE (Bâtiment MA)
Station 8 - CH-1015 - Lausanne - Switzerland

Fax: +41 21 69 32545

Time accurate partitioned algorithms for the solution of fluid-structure interaction problems in haemodynamics*

F. Nobile[1,2], M. Pozzoli[2], C. Vergara[3]

January 25, 2012

[1] CSQI-MATHICSE
École Polytechnique Fédérale de Lausanne, Switzerland
fabio.nobile@epfl.ch

[2] MOX– Modellistica e Calcolo Scientifico
Dipartimento di Matematica "F. Brioschi"
Politecnico di Milano, Italy
matteo1.pozzoli@mail.polimi.it

[3] Dipartimento di Ingegneria dell'Informazione e Metodi Matematici
Università di Bergamo, Italy
christian.vergara@polimi.it

Keywords: Fluid-structure interaction, blood flow, BDF schemes, time accuracy, partitioned schemes

Abstract

In this work we deal with the numerical solution of the fluid-structure interaction problem arising in the haemodynamic environment. In particular, we consider BDF and Newmark time discretization schemes, and we study different methods for the treatment of the fluid-structure interface position, focusing on partitioned algorithms for the prescription of the continuity conditions at the fluid-structure interface. We consider explicit and implicit algorithms, and new hybrid methods. We study numerically the performances and the accuracy of these schemes, highlighting the best solutions for haemodynamic applications. We also study numerically their convergence properties with respect to time discretization, by introducing an analytical test case.

*This work has been supported by the ERC Advanced Grant N.227058 MATHCARD

1 Introduction

Building efficient strategies for the solution of the fluid-structure interaction (FSI) problem is a major issue in *computational haemodynamics*. In particular here we are interested in the FSI problem arising by the interaction between the blood flow and the vessel wall deformation (see, e.g., [1, 2, 3, 4, 5, 6]). The main difficulties related to the numerical solution of the FSI problem are:

1. the treatment of the *interface position*, since the fluid domain is an unknown of the problem (*geometrical non-linearity*);

2. the treatment of the *interface continuity conditions*, which enforce continuity of velocities and normal stresses between fluid and structure;

3. the fact that the subproblems could be non-linear (*physical non-linearities*).

These features make the FSI problem a strongly non-linear coupled problem, as there is a substantial amount of energy exchanged between fluid and structure in each cardiac cycle.

Concerning the first point, we can mainly detect two strategies: an *implicit treatment* of the interface position, through, for example, fixed point or Newton iterations (see, e.g., [7, 8]), or an *explicit treatment*, by extrapolating the solution from previous time steps (see, e.g., [9, 10, 11]). Regarding the latter treatment, several theoretical results in the last ten years have shown that this strategy is able to guarantee the stability of related algorithms in the case of the linearized equations of infinitesimal elasticity, see, for example, [12, 13, 9, 11]. For what concerns the accuracy of such schemes, few results have been reported so far. We cite [14], where preliminary two-dimensional numerical results highlighted a good agreement with implicit solutions, and [15], where a convergence analysis has been provided. However, in the haemodynamic context, when dealing with three-dimensional real geometries and physiological data, it is still not clear whether the use of an explicit treatment of the FS interface is appropriate for practical purposes.

After a suitable linearization of the physical and geometrical non-linearities, whichever of the two strategies is adopted for the treatment of the interface position (implicit or explicit), one has to deal with a *linearized* FSI problem (in the sense that we have eliminated the geometrical and physical non-linearities). However, this problem is still coupled through the interface continuity conditions. For the solution of this linearized FSI problem, two strategies have been proposed and widely studied in the literature, namely the *monolithic* and the *partitioned* approaches. In the first case, the linearized problem is solved by building the whole FSI matrix, and then by solving the related linear system with a suitable preconditioned Krylov [7, 2], domain-decomposition [16] or multigrid [17, 18] method. Obviously, in this way the interface continuity conditions are automatically satisfied. Alternatively, in partitioned schemes one solves the fluid and structure subproblems in an iterative framework, until fulfillment of

the interface continuity conditions (see, e.g., [19, 20, 21, 22, 5]). Since we are interested in developing modular algorithms, which allow the use of pre-existing fluid and structure codes, we do not consider the monolithic approach here.

The first goal of this work is to compare the accuracy and performances of different treatments of the FS interface position, when partitioned procedures are considered for the enforcement of the continuity conditions. In particular, in this work we consider algorithms where, in general, two different iterative loops are peformed: one for the treatment of the geometrical and physical non-linearities, and another for the prescription of the interface continuity conditions. We study and compare implicit strategies, namely a "Double-loop" strategy where two nested loops are considered, a "Single-loop" strategy where only one loop is performed, and variants of these, called HS-n, where only an *a priori* fixed number of iterations on the continuity conditions are performed. The numerical results show that there is no significant differences between the two implicit schemes Double-loop and Single-loop (with a slight preference for Double-loop in terms of computational cost), whilst HS-n schemes, with n=2,3, are more efficient. This observations hold true both in the case of the linear infinitesimal and of the non-linear finite elasticity. Moreover, we consider inexact schemes, namely the geometric explicit strategy (GCIS-1) where only one iteration on the interface position per time step is performed [10, 16], and extensions of this, called GCIS-m schemes, where just an *a priori* fixed number of iterations on the interface position are performed. The related numerical results show that, in the case of the linear infinitesimal elasticity, GCIS-m schemes for $m = 1, 2, 3$, although not guaranteeing convergence to the interface conditions at each time step, preserve a good accuracy with a significant reduction in the CPU time with respect to implicit methods.

The second goal of the paper is to develop efficient ways to build high-order temporal schemes for the solution of the FSI problem. We consider the *Newmark scheme* for the structure in combination with the *theta-method* for the fluid, as well as BDF schemes up to fourth order for both subproblems. In particular, we study if suitable extrapolations of the interface quantities at each time step improve the time accuracy and/or reduce the number of iterations on the interface position. To do this, we propose an analytical test case for the FSI problem in the case of the linear infinitesimal elasticity.

The outline of the work is as follows. In Section 2 we introduce the FSI problem, its time discretization and a Lagrange multipliers-based formulation, useful for the derivation of the numerical schemes. In Section 3 we introduce and discuss the partitioned FSI algorithms. In Section 4 we show several 3D numerical results, in simplified and in real 3D geometries, both for the linear infinitesimal elasticity and for the non-linear finite elasticity. In Section 5 we propose the analytical test case to check the convergence properties of the schemes introduced, and we show related numerical results. Finally, in Section 6 we draw some conclusions.

2 The FSI problem and its time discretization

2.1 The continuous FSI problem

Let us consider an open domain $\Omega_f^t \subset \mathbb{R}^3$ like the one represented in Figure 1 (on the left). This represents the lumen of a vessel and it is function of time t. Inflow and outflow sections are denoted by $\Sigma_{f,i}^t$ (three in Figure 1). Blood

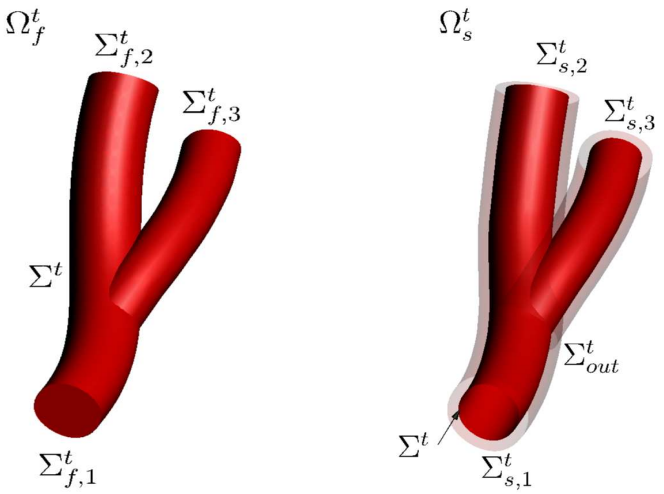

Figure 1: Representation of the domain of the FSI problem: fluid domain on the left, structure domain on the right.

velocity is denoted by $\boldsymbol{u}_f(\boldsymbol{x},t)$, the pressure by $p_f(\boldsymbol{x},t)$. The incompressible Navier-Stokes equations for a Newtonian fluid are assumed to hold in Ω_f^t. Let $\boldsymbol{T}_f$ be the related Cauchy stress tensor defined by

$$\boldsymbol{T}_f(\boldsymbol{u}_f, p_f) := -p_f \boldsymbol{I} + \mu(\nabla \boldsymbol{u}_f + (\nabla \boldsymbol{u}_f)^T).$$

Since we work in a moving domain, the fluid problem is stated in an *Arbitrary Lagrangian-Eulerian* (ALE) framework (see e.g. [23, 24]). The ALE map $\mathcal{A}$ is defined by an appropriate lifting of the structure displacement at the FS interface Σ^t, and defines the displacement of the points of the fluid domain $\boldsymbol{\eta}_m$ and their velocity $\boldsymbol{u}_m$. For any function v living in the current fluid configuration, we denote by $\widetilde{v} := v \circ \mathcal{A}$ its counterpart in the reference configuration. The ALE time derivative for a function $\boldsymbol{v}$ is defined as $\frac{D^A \boldsymbol{v}}{Dt} := \frac{\partial \widetilde{\boldsymbol{v}}}{\partial t} \circ \mathcal{A}^{-1}$, and the following identity holds

$$\frac{\partial \widetilde{\boldsymbol{v}}}{\partial t} = \frac{D^A \boldsymbol{v}}{Dt} - (\boldsymbol{u}_m \cdot \nabla)\boldsymbol{v}.$$

A classical choice in haemodynamic applications to define the ALE map is to consider a harmonic extension operator in the reference domain (see, e.g., [12]).

The vessel wall is denoted by Ω_s^t, which is an open subset of $\mathbb{R}^3$ (see Figure 1, right). The intersection of Ω_s^t and Ω_f^t is empty, and $\Sigma^t := \bar{\Omega}_s^t \cup \bar{\Omega}_f^t$. On Σ^t we define a normal unit vector $\boldsymbol{n}$ pointing outward of the solid domain and inward to the fluid domain. The inflow/outflow sections (three in Figure 1) are denoted by $\Sigma_{s,i}^t$. With Σ_{out}^t we denote the external surface of the structure domain. We denote by $\boldsymbol{\eta}_s(\boldsymbol{x}, t)$ the structure displacement, and by $\boldsymbol{T}_s = \boldsymbol{T}_s(\boldsymbol{\eta}_s)$ the Cauchy stress tensor for the structure. To describe the structure kinematics we adopt a purely Lagrangian approach, where $\mathcal{L}$ is the Lagrangian map. For any function g defined in the current solid configuration Ω_s^t, we denote by $\widetilde{g} := g \circ \mathcal{L}$ its counterpart in the reference domain. With this notation, we can write the Piola-Kirchhoff stress tensor $\widetilde{\boldsymbol{T}}_s$ in terms of the Cauchy tensor as $\widetilde{\boldsymbol{T}}_s(\widetilde{\boldsymbol{\eta}}_s) = J_s(\boldsymbol{\eta}_s)\boldsymbol{T}_s(\boldsymbol{\eta}_s)\boldsymbol{F}_s^{-T}(\boldsymbol{\eta}_s)$, where $\boldsymbol{F}_s := \nabla_{\boldsymbol{x}_s^0}\boldsymbol{x}_s^t$ is the deformation gradient with respect to the reference coordinates $\boldsymbol{x}_s^0$, $\boldsymbol{x}_s^t$ is the current coordinate, and $J_s := det(\boldsymbol{F}_s)$ is the local change of volume. The Piola-Kirchhoff stress tensor is related to the deformation gradient $\boldsymbol{F}_s$ by some linear or non-linear relation.

The strong formulation of the FSI problem, including the computation of the ALE map reads therefore as follows

1. *Fluid-Structure problem.* Given the (unknown) fluid domain velocity $\boldsymbol{u}_m$ and fluid domain Ω_f^t, find, at each time $t \in (0, T]$, fluid velocity $\boldsymbol{u}_f$, pressure p_f and structure displacement $\boldsymbol{\eta}_s$ such that

$$\begin{cases} \rho_f \dfrac{D^A \boldsymbol{u}_f}{Dt} + \rho_f((\boldsymbol{u}_f - \boldsymbol{u}_m)\cdot\nabla)\boldsymbol{u}_f - \nabla\cdot\boldsymbol{T}_f(\boldsymbol{u}_f, p_f) = \boldsymbol{f}_f & \text{in } \Omega_f^t, \\ \nabla\cdot\boldsymbol{u}_f = 0 & \text{in } \Omega_f^t, \\ \rho_s \dfrac{\partial^2\widetilde{\boldsymbol{\eta}}_s}{\partial t^2} + \mathcal{D}\left(\dfrac{\partial\widetilde{\boldsymbol{\eta}}_s}{\partial t}\right) - \nabla\cdot\widetilde{\boldsymbol{T}}_s(\widetilde{\boldsymbol{\eta}}_s) = \widetilde{\boldsymbol{f}}_s & \text{in } \Omega_s^0, \\ \boldsymbol{u}_f = \dfrac{\partial\boldsymbol{\eta}_s}{\partial t} & \text{on } \Sigma^t, \\ \boldsymbol{T}_s(\boldsymbol{\eta}_s)\,\boldsymbol{n} - \boldsymbol{T}_f(\boldsymbol{u}_f, p_f)\,\boldsymbol{n} = \boldsymbol{0} & \text{on } \Sigma^t, \\ \alpha_e\widetilde{\boldsymbol{\eta}}_s + \widetilde{\boldsymbol{T}}_s(\widetilde{\boldsymbol{\eta}}_s)\,\widetilde{\boldsymbol{n}} = P_{ext}\widetilde{\boldsymbol{n}}, & \text{on } \Sigma_{out}^0, \end{cases} \tag{1}$$

   where $\mathcal{D}$ is a linear dumping operator, ρ_f and ρ_s are the fluid and structure densities, μ is the constant blood viscosity, $\boldsymbol{f}_f$ and $\boldsymbol{f}_s$ the forcing terms;

2. *Geometry problem.* Given the (unknown) interface structure displacement $\widetilde{\boldsymbol{\eta}}_s|_{\Sigma^0}$, find the displacement of the points of the fluid domain $\boldsymbol{\eta}_m$ such that

$$\begin{cases} -\triangle\widetilde{\boldsymbol{\eta}}_m = \boldsymbol{0} & \text{on } \Omega_f^0, \\ \widetilde{\boldsymbol{\eta}}_m = \widetilde{\boldsymbol{\eta}}_s & \text{on } \Sigma^0, \end{cases} \tag{2}$$

   and then find accordingly the fluid domain velocity $\widetilde{\boldsymbol{u}}_m := \frac{\partial\widetilde{\boldsymbol{\eta}}_m}{\partial t}$, and the new points $\boldsymbol{x}_f^t$ of the fluid domain by moving the points $\boldsymbol{x}_f^0$ of the reference domain Ω_f^0:

$$\boldsymbol{x}_f^t = \boldsymbol{x}_f^0 + \widetilde{\boldsymbol{\eta}}_m.$$

The two matching conditions enforced at the interface are the *continuity of velocities* $(1)_4$ and the *continuity of normal stresses* $(1)_5$. The fluid and structure are also coupled by the geometry problem, leading to a highly non-linear system of partial differential equations. Equations (1) and (2) have to be endowed with suitable boundary conditions on $\Omega_f^t \setminus \Sigma^t$ and $\Omega_s^0 \setminus (\Sigma^0 \cup \Sigma_{out}^0)$, and with suitable initial conditions. We prescribe the Robin boundary condition $(1)_6$ on Σ_{out}^0, with the aim of modeling the presence of a surrounding tissue around the vessel. This choice corresponds to modeling this tissue as a perfectly elastic body, with α_e the corresponding elastic coefficient (see [25, 26]).

2.2 Time discretization of the FSI problem

Let Δt be the time discretization parameter and $t^n := n\,\Delta t$, $n = 0, 1, \ldots$. For a generic function z, we denote with z^n the approximation of $z(t^n)$. In this work we consider two families of schemes, namely the *Backward Differentiation Formulae* (BDF) schemes (see [27, 28]) and the family obtained by the *Newmark* schemes for the structure, and the *theta-methods* for the fluid. We propose here a unified formulation of the time discrete problem (1)-(2), that accommodates both families of schemes.

1. *Fluid-Structure problem.* Given the (unknown) fluid domain velocity $\boldsymbol{u}_m^{n+1}$ and fluid domain Ω_f^{n+1}, the parameters $\beta_{f,i} (i = 0, \ldots, q)$, χ_f, $\beta_{s,i} (i = 0, \ldots, q)$, σ_s, ζ_s, $\xi_{s,i} (i = 0, \ldots, q+1)$, χ_s, κ_s, the solution at previous time steps, and functions $\boldsymbol{f}_f^{n+1}$, $\boldsymbol{f}_s^{n+1}$ and P_{ext}, find fluid velocity $\boldsymbol{u}_f^{n+1}$, pressure p_f^{n+1} and structure displacement $\boldsymbol{\eta}_s^{n+1}$ such that

$$
\begin{cases}
\rho_f \dfrac{\beta_{f,0}}{\Delta t} \boldsymbol{u}_f^{n+1} + \rho_f ((\boldsymbol{u}_f^{n+1} - \boldsymbol{u}_m^{n+1}) \cdot \nabla) \boldsymbol{u}_f^{n+1} & \\
\qquad\qquad -\nabla \cdot \boldsymbol{T}_f^{n+1}(\boldsymbol{u}_f^{n+1}, p_f^{n+1}) = \boldsymbol{f}_f^{n+1} + \rho_f \boldsymbol{f}_{f,W}^{n+1} & \text{in } \Omega_f^{n+1}, \\
\nabla \cdot \boldsymbol{u}_f^{n+1} = 0 & \text{in } \Omega_f^{n+1}, \\
\rho_s \dfrac{\xi_{s,0}}{\Delta t^2} \widetilde{\boldsymbol{\eta}}_s^{n+1} + \mathcal{D}\left(\dfrac{\beta_{s,0}}{\Delta t} \widetilde{\boldsymbol{\eta}}_s^{n+1} \right) - \nabla \cdot \widetilde{\boldsymbol{T}}_s^{n+1}(\widetilde{\boldsymbol{\eta}}_s^{n+1}) & \\
\qquad\qquad = \widetilde{\boldsymbol{f}}_s^{n+1} + \mathcal{D}\left(\widetilde{\boldsymbol{f}}_{s,U}^{n+1} \right) + \rho_s \widetilde{\boldsymbol{f}}_{s,W}^{n+1} & \text{in } \Omega_s^0, \\
\boldsymbol{u}_f^{n+1} = \boldsymbol{u}_s^{n+1} & \text{on } \Sigma^{n+1}, \\
\boldsymbol{T}_s^{n+1}(\boldsymbol{\eta}_s^{n+1})\, \boldsymbol{n} - \boldsymbol{T}_f^{n+1}(\boldsymbol{u}_f^{n+1}, p_f^{n+1})\, \boldsymbol{n} = \boldsymbol{0} & \text{on } \Sigma^{n+1}, \\
\alpha_e \widetilde{\boldsymbol{\eta}}_s^{n+1} + \widetilde{\boldsymbol{T}}_s^{n+1}(\widetilde{\boldsymbol{\eta}}_s^{n+1})\, \widetilde{\boldsymbol{n}} = P_{ext} \widetilde{\boldsymbol{n}} & \text{on } \Sigma_{out}^0,
\end{cases}
\tag{3}
$$

where

	BDF	Newmark/theta-methods
$\boldsymbol{f}_{s,U}^{n+1} :=$	$\displaystyle\sum_{i=1}^{q} \frac{\beta_{s,i}}{\Delta t}\boldsymbol{\eta}_s^{n+1-i}$	$\displaystyle\frac{\beta_{s,1}}{\Delta t}\boldsymbol{\eta}_s^n + \chi_s \boldsymbol{u}_s^n + \Delta t \kappa_s \boldsymbol{w}_s^n,$
$\boldsymbol{f}_{s,W}^{n+1} :=$	$\displaystyle\sum_{i=1}^{q+1} \frac{\xi_{s,i}}{\Delta t^2}\boldsymbol{\eta}_s^{n+1-i}$	$\displaystyle\frac{\xi_{s,1}}{\Delta t^2}\boldsymbol{\eta}_s^n + \frac{\sigma_s}{\Delta t}\boldsymbol{u}_s^n + \zeta_s \boldsymbol{w}_s^n,$
$\boldsymbol{f}_{f,W}^{n+1} :=$	$\displaystyle\sum_{i=1}^{q} \frac{\beta_{f,i}}{\Delta t}\boldsymbol{u}_f^{n+1-i}$	$\displaystyle\frac{\beta_{f,1}}{\Delta t}\boldsymbol{u}_f^n + \chi_f \boldsymbol{w}_f^n,$

are the forcing terms coming from the time discretization, and q is a fixed number which defines the number of steps of BDF methods. In problem (3) we have also introduced the structure velocity $\boldsymbol{u}_s^n := \frac{\beta_{s,0}}{\Delta t}\boldsymbol{\eta}_s^n - \boldsymbol{f}_{s,U}^n$, the structure acceleration $\boldsymbol{w}_s^n := \frac{\xi_{s,0}}{\Delta t^2}\boldsymbol{\eta}_s^n - \boldsymbol{f}_{s,W}^n$, and the fluid acceleration $\boldsymbol{w}_f^n := \frac{\beta_{f,0}}{\Delta t}\boldsymbol{u}_f^n - \boldsymbol{f}_{f,W}^n$. In Section 4 we provide concrete values for different sets of these parameters.

2. *Geometry problem.* Given the (unknown) interface structure displacement $\widetilde{\boldsymbol{\eta}}_s^{n+1}|_{\Sigma^0}$, solve a harmonic extension problem

$$\begin{cases} -\triangle \widetilde{\boldsymbol{\eta}}_m^{n+1} = \boldsymbol{0} & \text{in } \Omega_f^0, \\ \widetilde{\boldsymbol{\eta}}_m^{n+1} = \widetilde{\boldsymbol{\eta}}_s^{n+1} & \text{on } \Sigma^0, \end{cases} \tag{4}$$

and then find accordingly the discrete fluid domain velocity $\widetilde{\boldsymbol{u}}_m^{n+1}$ and the points $\boldsymbol{x}_f^{n+1}$ of the new fluid domain by

$$\widetilde{\boldsymbol{u}}_m^{n+1} := \frac{\beta_{s,0}}{\Delta t}\widetilde{\boldsymbol{\eta}}_m^{n+1} - \widetilde{\boldsymbol{f}}_{m,U}^{n+1}, \qquad \boldsymbol{x}_f^{n+1} = \boldsymbol{x}_f^0 + \widetilde{\boldsymbol{\eta}}_m^{n+1}. \tag{5}$$

Here $\widetilde{\boldsymbol{f}}_{m,U}^{n+1}$, $\widetilde{\boldsymbol{w}}_m^{n+1}$ and $\widetilde{\boldsymbol{f}}_{m,W}^{n+1}$ (the last two quantities are needed for the computation of $\widetilde{\boldsymbol{f}}_{m,U}^{n+1}$) are obtained using the same formulae as for $\boldsymbol{f}_{s,U}$, $\boldsymbol{w}_s$ and $\boldsymbol{f}_{s,W}$. Observe that $(4)_2$ guarantees that the displacement of the fluid interface coincides with that of the structure (geometrical conformity), whereas (5) guarantees that also the mesh and structure velocities coincide at the FS interface. The parameters introduced in the definitions of the forcing terms, of the structure velocity and of the accelerations, define completely the schemes. BDF schemes are exactly of order q, and we consider $q = 1, 2, 3, 4$, whilst Newmark/theta-method schemes are in general of order 1, becoming of order 2 for example for the particular choice *Midpoint/Crank-Nicolson*, which is the one considered in this work (see Section 4.2). The overall order of the FSI problem is then expected to be that of the two subproblems, although no proofs are available so far in the literature, at the best of our knowledges.

2.3 A Lagrange multipliers-based formulation

In order to introduce suitable algorithms for the numerical solution of (3) and (4), we consider here an equivalent formulation based on the introduction of

three Lagrange multipliers living at the FS interface, representing the fluid and structure normal stresses $\boldsymbol{\lambda}_f$ and $\boldsymbol{\lambda}_s$, and the normal derivative of the fluid mesh displacement $\boldsymbol{\lambda}_m$ (see the end of this section). These new unknowns are introduced just to simplify the expression of the three interface continuity conditions $(3)_{4-5}$ and $(4)_2$, and the derivation of the partitioned algorithms. However, we have not introduced them in our practical implementation of the algorithms to avoid extra costs.

We start by introducing some new notations. For the sake of notation we remove the temporal index $^{n+1}$. Given a space W, we denote with W^* its dual, with Σ_f^D and Σ_m^D we denote the parts of the boundary $\partial\Omega_f \setminus \Sigma$ where Dirichlet boundary conditions are prescribed for the fluid subproblem and for the harmonic extension problem, respectively, and with $\Sigma_s^{D,0}$ the part of $\partial\Omega_s^0 \setminus \Sigma^0$ where Dirichlet conditions are prescribed for the structure subproblem. Then, we define the following spaces

$$V_f := \{v \in H^1(\Omega_f) : v|_{\Sigma_f^D} = 0\}, \qquad Q := L^2(\Omega_f)^1,$$

$$V_s := \{v \in H^1(\Omega_s^0) : v|_{\Sigma_s^{D,0}} = 0\}, \qquad V_m := \{v \in H^1(\Omega_f^0) : v|_{\Sigma_m^{D,0}} = 0\}.$$

Let $\boldsymbol{v}_f := (\boldsymbol{u}_f, p_f)$ collect the fluid unknowns and $\mathcal{F} : [V_f]^3 \times Q \times [V_m]^3 \to ([V_f]^3 \times Q)^*$ be the fluid operator, defined by

$$< \mathcal{F}(\boldsymbol{v}_f, \boldsymbol{u}_m), (\boldsymbol{v}, q) >:=$$

$$\int_{\Omega_f} \left[\left(\rho_f \frac{\beta_{f,0}}{\Delta t} \boldsymbol{u}_f + \rho_f((\boldsymbol{u}_f - \boldsymbol{u}_m) \cdot \nabla)\boldsymbol{u}_f \right) \cdot \boldsymbol{v} + \boldsymbol{T}_f(\boldsymbol{v}_f) : \nabla \boldsymbol{v} - \nabla \cdot \boldsymbol{u}_f \, q \right] d\boldsymbol{x},$$

with $(\boldsymbol{v}, q) \in [V_f]^3 \times Q$, and let $\mathcal{G}_f$ be the operator related to the right hand side of the fluid momentum equation, that is

$$< \mathcal{G}_f, (\boldsymbol{v}, q) >:= \int_{\Omega_f} \left(\boldsymbol{f}_f^{n+1} + \rho_f \boldsymbol{f}_{f,W}^{n+1} \right) \cdot \boldsymbol{v} \, d\boldsymbol{x}.$$

Analogously, for the structure subproblem we define the operator $\mathcal{S} : [V_s]^3 \to ([V_s]^3)^*$ as follows

$$< \mathcal{S}(\widetilde{\boldsymbol{\eta}}_s), \widetilde{\boldsymbol{\mu}} >:= \int_{\Omega_s^0} \left[\left(\rho_s \frac{\xi_{s,0}}{\Delta t^2} \widetilde{\boldsymbol{\eta}}_s + \mathcal{D}\left(\frac{\beta_{s,0}}{\Delta t} \widetilde{\boldsymbol{\eta}}_s \right) \right) \cdot \widetilde{\boldsymbol{\mu}} + \widetilde{\boldsymbol{T}}_s(\widetilde{\boldsymbol{\eta}}_s) : \nabla \widetilde{\boldsymbol{\mu}} \right] d\widetilde{\boldsymbol{x}},$$

with $\widetilde{\boldsymbol{\mu}} \in [V_s]^3$, and $\mathcal{G}_s$ as follows

$$< \mathcal{G}_s, \widetilde{\boldsymbol{\mu}} >:= \int_{\Omega_s^0} \left(\widetilde{\boldsymbol{f}}_s^{n+1} + \mathcal{D}(\widetilde{\boldsymbol{f}}_{s,U}^{n+1}) + \rho_s \widetilde{\boldsymbol{f}}_{s,W}^{n+1} \right) \cdot \widetilde{\boldsymbol{\mu}} \, d\widetilde{\boldsymbol{x}},$$

[1]Since we solve the FSI problem in a partitioned way with Robin conditions at the FS interface (see (9)), the pressure is always defined and $L^2(\Omega_f)$ is the suitable pressure space for the weak formulation.

with $\widetilde{\boldsymbol{\mu}} \in [V_s]^3$. Finally, for the harmonic extension, we introduce the operator $\mathcal{H} : [V_m]^3 \to ([V_m]^3)^*$ defined as

$$< \mathcal{H}\,\widetilde{\boldsymbol{\eta}}_m, \widetilde{\boldsymbol{z}} >:= \int_{\Omega_f^0} \nabla\widetilde{\boldsymbol{\eta}}_m : \nabla\widetilde{\boldsymbol{z}}\, d\boldsymbol{x}^0,$$

with $\widetilde{\boldsymbol{z}} \in [V_m]^3$. We also define the following trace operators

$$\begin{array}{l} \widetilde{\gamma}_f : [V_f]^3 \times Q \to [H^{1/2}(\Sigma^0)]^3,\ \widetilde{\gamma}_f(\boldsymbol{v}, q) := \widetilde{\boldsymbol{v}}|_{\Sigma^0}\,, \\ \widetilde{\gamma}_s : [V_s]^3 \to [H^{1/2}(\Sigma^0)]^3,\ \widetilde{\gamma}_s\widetilde{\boldsymbol{\mu}} := \widetilde{\boldsymbol{\mu}}|_{\Sigma^0}\,, \\ \widetilde{\gamma}_m : [V_m]^3 \to [H^{1/2}(\Sigma^0)]^3,\ \widetilde{\gamma}_m\widetilde{\boldsymbol{z}} := \widetilde{\boldsymbol{z}}|_{\Sigma^0}\,, \end{array} \tag{6}$$

and the related adjoint operators as follows

$$\begin{array}{l} \widetilde{\gamma}_f^* : [H^{-1/2}(\Sigma^0)]^3 \to \left([V_f]^3 \times Q\right)^*,\ < \widetilde{\gamma}_f^*\widetilde{\boldsymbol{\lambda}}, (\boldsymbol{v}, q) >:=< \widetilde{\boldsymbol{\lambda}}, \widetilde{\gamma}_f(\boldsymbol{v}, q) >\ \ \forall (\boldsymbol{v}, q) \in [V_f]^3 \times Q, \\ \widetilde{\gamma}_s^* : [H^{-1/2}(\Sigma^0)]^3 \to \left([V_s]^3\right)^*,\ < \widetilde{\gamma}_s^*\widetilde{\boldsymbol{\lambda}}, \widetilde{\boldsymbol{\mu}} >:=< \widetilde{\boldsymbol{\lambda}}, \widetilde{\gamma}_s\widetilde{\boldsymbol{\mu}} >\ \ \forall \widetilde{\boldsymbol{\mu}} \in [V_s]^3, \\ \widetilde{\gamma}_m^* : [H^{-1/2}(\Sigma^0)]^3 \to \left([V_m]^3\right)^*,\ < \widetilde{\gamma}_m^*\widetilde{\boldsymbol{\lambda}}, \widetilde{\boldsymbol{z}} >:=< \widetilde{\boldsymbol{\lambda}}, \widetilde{\gamma}_m\widetilde{\boldsymbol{z}} >\ \ \forall \widetilde{\boldsymbol{z}} \in [V_m]^3. \end{array} \tag{7}$$

For functions regular enough, from previous definitions we have

$$< \widetilde{\gamma}_f^*\widetilde{\boldsymbol{\lambda}}, (\boldsymbol{v}, q) >= \int_{\Sigma^0} \widetilde{\boldsymbol{\lambda}} \cdot \widetilde{\boldsymbol{v}}\, d\sigma^0, \quad < \widetilde{\gamma}_s^*\widetilde{\boldsymbol{\lambda}}, \widetilde{\boldsymbol{\mu}} >= \int_{\Sigma^0} \widetilde{\boldsymbol{\lambda}} \cdot \widetilde{\boldsymbol{\mu}}\, d\sigma^0, \quad < \widetilde{\gamma}_m^*\widetilde{\boldsymbol{\lambda}}, \widetilde{\boldsymbol{z}} >= \int_{\Sigma^0} \widetilde{\boldsymbol{\lambda}} \cdot \widetilde{\boldsymbol{z}}\, d\sigma^0. \tag{8}$$

We observe that the trace operator for fluid quantities returns the trace in the *reference configuration*.

We are now ready to rewrite problem (3)-(4) as follows

$$\left\{ \begin{array}{rcll} \mathcal{H}\,\widetilde{\boldsymbol{\eta}}_m + \widetilde{\gamma}_m^*\widetilde{\boldsymbol{\lambda}}_m &=& \boldsymbol{0} & \text{in } \left([V_m]^3\right)^*, \\ \widetilde{\gamma}_m\widetilde{\boldsymbol{\eta}}_m &=& \widetilde{\gamma}_s\widetilde{\boldsymbol{\eta}}_s & \text{on } \Sigma^0, \\ \mathcal{F}(\boldsymbol{v}_f, \boldsymbol{u}_m) + \widetilde{\gamma}_f^*\widetilde{\boldsymbol{\lambda}}_f &=& \mathcal{G}_f & \text{in } \left([V_f]^3 \times Q\right)^*, \\ \alpha_f\,\widetilde{\gamma}_f\boldsymbol{v}_f + \widetilde{\boldsymbol{\lambda}}_f &=& \alpha_f\widetilde{\gamma}_s\left(\frac{\beta_{s,0}}{\Delta t}\widetilde{\boldsymbol{\eta}}_s - \widetilde{\boldsymbol{f}}_{s,U}\right) - \widetilde{\boldsymbol{\lambda}}_s & \text{on } \Sigma^0, \\ \alpha_s\frac{\beta_{s,0}}{\Delta t}\,\widetilde{\gamma}_s\widetilde{\boldsymbol{\eta}}_s + \widetilde{\boldsymbol{\lambda}}_s &=& \alpha_s\widetilde{\gamma}_f\boldsymbol{v}_f - \widetilde{\boldsymbol{\lambda}}_f + \alpha_s\widetilde{\gamma}_s\widetilde{\boldsymbol{f}}_{s,U} & \text{on } \Sigma^0, \\ \mathcal{S}(\widetilde{\boldsymbol{\eta}}_s) + \widetilde{\gamma}_s^*\widetilde{\boldsymbol{\lambda}}_s &=& \mathcal{G}_s & \text{in } \left([V_s]^3\right)^*, \end{array} \right. \tag{9}$$

where the interface continuity conditions $(9)_{4-5}$ are linear combinations of conditions $(3)_{4-5}$, through the introduction of two functions in $L^\infty(\Sigma^0)$, $\alpha_f \neq \alpha_s$. This will be useful to derive partitioned procedures based on Robin interface conditions (Robin-Robin (RR) schemes, see [5, 29, 30, 31]). This approach has good convergence properties, independent of the added-mass effect (which is very high in haemodynamic contexts, see [20]) when the parameters α_f and α_s are suitably chosen, as shown in [5, 31]. Moreover, we point out that these conditions together with $(9)_2$ are written in the *reference configuration*. This choice will simplify the computation of derivatives in the Newton method, as it will be clear in the next section.

We give now a characterization of the Lagrange multipliers introduced. From the definition of $\mathcal{F}$, by taking $\boldsymbol{v}$ as a divergence free extension of a function $\boldsymbol{\phi} \in [H^{1/2}(\Sigma)]^3$, zero on Σ_f^D, and integrating by parts, we have

$$0 =< -\mathcal{G}_f + \mathcal{F}(\boldsymbol{v}_f, \boldsymbol{u}_m), (\boldsymbol{v}, 0) > + < \widetilde{\gamma}_f^* \widetilde{\boldsymbol{\lambda}}_f, (\boldsymbol{v}, 0) >= -\int_\Sigma \boldsymbol{T}_f(\boldsymbol{v}_f)\, \boldsymbol{n} \cdot \boldsymbol{\phi}\, d\sigma + < \widetilde{\boldsymbol{\lambda}}_f, \widetilde{\gamma}_f(\boldsymbol{v}, 0) > .$$

If $\boldsymbol{\lambda}_f$ is regular enough, we obtain thanks to (8)

$$-\int_\Sigma \boldsymbol{T}_f(\boldsymbol{v}_f)\, \boldsymbol{n} \cdot \boldsymbol{\phi}\, d\sigma + < \widetilde{\boldsymbol{\lambda}}_f, \widetilde{\gamma}_f(\boldsymbol{v}, 0) >= -\int_\Sigma \boldsymbol{T}_f(\boldsymbol{v}_f)\, \boldsymbol{n} \cdot \boldsymbol{\phi}\, d\sigma + \int_{\Sigma^0} \widetilde{\boldsymbol{\lambda}}_f \cdot \widetilde{\boldsymbol{\phi}}\, d\sigma^0 = 0.$$

We introduce now the quantities $\boldsymbol{F}_{ALE} := \nabla_{\boldsymbol{x}_f^0} \boldsymbol{x}_f$, and $J_{ALE} := det(\boldsymbol{F}_{ALE})$. Then, from the Nanson formula $\boldsymbol{n}\, d\sigma = J_{ALE} \boldsymbol{F}_{ALE}^{-T} \widetilde{\boldsymbol{n}}\, d\sigma^0$, we obtain

$$-\int_{\Sigma^0} J_{ALE} \boldsymbol{T}_f(\boldsymbol{v}_f) \boldsymbol{F}_{ALE}^{-T} \widetilde{\boldsymbol{n}} \cdot \widetilde{\boldsymbol{\phi}}\, d\sigma^0 + \int_{\Sigma^0} \widetilde{\boldsymbol{\lambda}}_f \cdot \widetilde{\boldsymbol{\phi}}\, d\sigma^0 = 0.$$

Since the previous identity holds for all $\boldsymbol{\phi} \in [H^{1/2}(\Sigma)]^3$, we obtain

$$\widetilde{\boldsymbol{\lambda}}_f = \left(J_{ALE}\, \boldsymbol{T}_f(\boldsymbol{v}_f) \boldsymbol{F}_{ALE}^{-T} \widetilde{\boldsymbol{n}} \right)\Big|_{\Sigma^0} = \left(\widetilde{\boldsymbol{T}}_f(\widetilde{\boldsymbol{v}}_f) \widetilde{\boldsymbol{n}} \right)\Big|_{\Sigma^0},$$

which shows that the Lagrange multiplier $\boldsymbol{\lambda}_f$ has the physical meaning of the fluid normal stress at the FS interface *in the reference configuration*. With analogous steps, we obtain

$$\widetilde{\boldsymbol{\lambda}}_s = -\left(\widetilde{\boldsymbol{T}}_s(\widetilde{\boldsymbol{\eta}}_s) \widetilde{\boldsymbol{n}} \right)\Big|_{\Sigma^0}, \qquad \widetilde{\boldsymbol{\lambda}}_m = \left. \frac{\partial \widetilde{\boldsymbol{\eta}}_m}{\partial \widetilde{\boldsymbol{n}}} \right|_{\Sigma^0}.$$

3 Numerical algorithms

For the solution of the FSI problem (9), we propose to use a general preconditioned Richardson method

$$\widehat{F}(y^k)\, \delta y^{k+1} = -F(y^k), \tag{10}$$

where y^k denotes the FSI solution $[\widetilde{\boldsymbol{\eta}}_m^k, \widetilde{\boldsymbol{\lambda}}_m^k, \boldsymbol{v}_f^k, \widetilde{\boldsymbol{\lambda}}_f^k, \widetilde{\boldsymbol{\lambda}}_s^k, \widetilde{\boldsymbol{\eta}}_s^k]$ at the generic subiteration k, δy^{k+1} is the increment of the FSI solution at the new iteration $k+1$ with respect to y^k, $F(y) = 0$ corresponds to problem (9), and $\widehat{F}$ is a suitable preconditioner.

We consider here quasi-Newton preconditioners, derived by the Newton method which is given by (10) with

$$\widehat{F} = \nabla F = \left[\begin{array}{cc|cc|cc} \mathcal{H} & \widetilde{\gamma}_m^* & & & & -\widetilde{\gamma}_s \\ \widetilde{\gamma}_m & & & & & \\ \hline \nabla_{u_m}\mathcal{F} & & \nabla_{v_f}\mathcal{F} & \widetilde{\gamma}_f^* & & \\ & & \alpha_f \widetilde{\gamma}_f & I & I & -\alpha_f \frac{\beta_{s,0}}{\Delta t} \widetilde{\gamma}_s \\ \hline & & -\alpha_s \widetilde{\gamma}_f & I & I & \alpha_s \frac{\beta_{s,0}}{\Delta t} \widetilde{\gamma}_s \\ & & & & \widetilde{\gamma}_s^* & \nabla_{\eta_s}\mathcal{S} \end{array}\right].$$

This is obtained by taking only *material derivatives*, i.e. the differentiation is done with respect to the unknowns in the *reference configuration*. By doing this, the trace operators introduced in (6) and (7) are *linear* and the differentiation of the interface conditions becomes trivial. We point out however that the operator $\mathcal{F}$ heavily depends on the unknown ALE mapping $\boldsymbol{\eta}_m$ and this introduces *shape derivatives* in the term $\nabla_{u_m}\mathcal{F}$.

We are ready now to derive from ∇F quasi-Newton preconditioners $\widehat{F}$, leading to suitable algorithms for the numerical solution of (9). In all these preconditioners, we consider an approximation of $\nabla_{v_f}\mathcal{F}$ given by $\widehat{\nabla}_{v_f}\mathcal{F}\,\delta\boldsymbol{v}_f := \begin{cases} \rho_f \dfrac{\beta_{f,0}}{\Delta t}\delta\boldsymbol{u}_f + \rho_f((\boldsymbol{u}_f-\boldsymbol{u}_m)\cdot\nabla)\delta\boldsymbol{u}_f - \nabla\cdot\boldsymbol{T}_f(\delta\boldsymbol{u}_f,\delta p_f) \\ \nabla\cdot\delta\boldsymbol{u}_f \end{cases}$, that is we skip the term $(\delta\boldsymbol{u}_f\cdot\nabla)\boldsymbol{u}_f$. For practical reasons, in the following algorithms this problem will be written in non incremental form. Moreover, in order to make clearer its expression, we will indicate explicitly the convective term at hand, $\boldsymbol{w}$, as follows: $\widehat{\nabla}_{v_f}\mathcal{F}(\boldsymbol{w})\boldsymbol{v}_f$. Finally, in the proposed preconditioners we will not consider the shape derivatives $\nabla_{u_m}\mathcal{F}$.

The stopping criterion is given by the computation of the residual $F(y)$, that is

$$\|F(y^{k+1})\|_Y \le \varepsilon_1 + \varepsilon_2\|y_R^{k+1}\|_Y,$$

where Y is the global space where the solution y belongs to and ε_1 and ε_2 are given tolerances. We observe that in the previous definition we use both an absolute and a relative criterion, so that we say that convergence is achieved when both criteria are satisfied. In particular, the normalization is done with respect to the term y_R, which is properly chosen case by case. By considering (10), an equivalent stopping criterion (more useful from the practical point of view) is

$$\|F(y^{k+1}) - \widehat{F}(y^k)\delta y^{k+1} - F(y^k)\|_Y \le \varepsilon_1 + \varepsilon_2\|y_R^{k+1}\|_Y. \tag{11}$$

3.1 Single-loop scheme

We consider the following *three blocks Gauss-Seidel* preconditioner (see also [16])

$$\widehat{J}_{SL} = \left[\begin{array}{cc|cc|cc} \mathcal{H} & \widetilde{\gamma}_m^* & & & & \\ \widetilde{\gamma}_m & & & & & \\ \hline & & \widehat{\nabla}_{v_f}\mathcal{F} & \widetilde{\gamma}_f^* & & \\ & & \alpha_f\widetilde{\gamma}_f & I & & \\ \hline & & -\alpha_s\widetilde{\gamma}_f & I & I & \alpha_s\frac{\beta_{s,0}}{\Delta t}\widetilde{\gamma}_s \\ & & & & \widetilde{\gamma}_s^* & \nabla_{\eta_s}\mathcal{S} \end{array}\right],$$

which corresponds to the sequential solution of the harmonic extension, fluid subproblem and structure subproblem, leading to the following algorithm:

Given the solution at iteration k, solve at the current iteration $k+1$ until convergence

1. The harmonic extension

$$\begin{cases} \mathcal{H}\,\widetilde{\boldsymbol{\eta}}_m^{k+1} + \widetilde{\gamma}_m^* \widetilde{\boldsymbol{\lambda}}_m^{k+1} = 0 & \text{in } \left([V_m]^3\right)^*, \\ \widetilde{\gamma}_m \widetilde{\boldsymbol{\eta}}_m^{k+1} = \widetilde{\gamma}_s \widetilde{\boldsymbol{\eta}}_s^k & \text{on } \Sigma^0, \end{cases}$$

obtaining the new fluid domain Ω_f^{k+1} and the fluid domain velocity $\boldsymbol{u}_m^{k+1}$ by using (5).

2. The fluid subproblem with a Robin condition at the FS interface

$$\begin{cases} \widehat{\nabla}_{v_f} \mathcal{F}(\boldsymbol{u}_f^k - \boldsymbol{u}_m^{k+1})\, \boldsymbol{v}_f^{k+1} + \widetilde{\gamma}_f^* \widetilde{\boldsymbol{\lambda}}_f^{k+1} = \mathcal{G}_f & \text{in } \left([V_f^{k+1}]^3 \times Q^{k+1}\right)^*, \\ \alpha_f \gamma_f \boldsymbol{v}_f^{k+1} + \boldsymbol{\lambda}_f^{k+1} = \alpha_f \gamma_s \left(\frac{\beta_{s,0}}{\Delta t} \boldsymbol{\eta}_s^k - \boldsymbol{f}_{s,U}\right) - \boldsymbol{\lambda}_s^k & \text{on } \Sigma^{k+1}, \end{cases} \tag{12}$$

3. The structure subproblem with a Robin condition at the FS interface

$$\begin{cases} \nabla_\eta \mathcal{S}(\widetilde{\boldsymbol{\eta}}_s^k)\, \delta\widetilde{\boldsymbol{\eta}}_s^{k+1} + \widetilde{\gamma}_s^* \delta\widetilde{\boldsymbol{\lambda}}_s^{k+1} = \mathcal{G}_s - \mathcal{S}(\widetilde{\boldsymbol{\eta}}_s^k) - \widetilde{\gamma}_s^* \widetilde{\boldsymbol{\lambda}}_s^k & \text{in } \left([V_s]^3\right)^*, \\ \alpha_s \dfrac{\beta_{s,0}}{\Delta t}\, \widetilde{\gamma}_s\, \widetilde{\boldsymbol{\eta}}_s^{k+1} - \widetilde{\boldsymbol{\lambda}}_s^{k+1} = \alpha_s \widetilde{\gamma}_f\, \widetilde{\boldsymbol{v}}_f^{k+1} - \widetilde{\boldsymbol{\lambda}}_f^{k+1} + \alpha_s \widetilde{\gamma}_s \widetilde{\boldsymbol{f}}_{s,U} & \text{on } \Sigma^0. \end{cases}$$

Here $\gamma_f : [V_f]^3 \times Q \to H^{1/2}(\Sigma)$ and $\gamma_s : [V_s]^3 \to H^{1/2}(\Sigma)$ are the trace operators defined on the deformed interface, as $\gamma_f(\boldsymbol{v}, q) := \boldsymbol{v}|_\Sigma$, $(\boldsymbol{v}, q) \in [V_f]^3 \times Q$ and $\gamma_s \boldsymbol{v} := \boldsymbol{v}|_\Sigma$, $\boldsymbol{v} \in [V_s]^3$, respectively. We observe that the Robin condition in the structure subproblem has been written in non-incremental form since it is linear.

Remark **1** *We observe that the momentum equation in* $(12)_1$ *coincides with an Oseen problem where the convective term is given by* $\boldsymbol{u}_f^k - \boldsymbol{u}_m^{k+1}$. *In particular, we have the following momentum equation*

$$\rho_f \frac{\beta_{f,0}}{\Delta t} \boldsymbol{u}_f^{k+1} + \rho_f((\boldsymbol{u}_f^k - \boldsymbol{u}_m^{k+1}) \cdot \nabla)\boldsymbol{u}_f^{k+1} - \nabla \cdot \boldsymbol{T}_f(\boldsymbol{u}_f^{k+1}, p_f^{k+1}) = \boldsymbol{f}_f + \rho_f \boldsymbol{f}_{f,W} \quad \text{in } \Omega_f^{k+1}.$$

We observe the use of the velocity fluid domain at the current iteration in the convective term, according to a Gauss-Seidel preconditioner philosophy. □

From (11), we obtain the following stopping criterion

$$\|\widetilde{\gamma}_s\, \widetilde{\boldsymbol{\eta}}_s^{k+1} - \widetilde{\gamma}_s\, \widetilde{\boldsymbol{\eta}}_s^k\|_X + \|((\boldsymbol{u}_f^{k+1} - \boldsymbol{u}_f^k) \cdot \nabla)\, \boldsymbol{u}_f^{k+1}\|_W \tag{13}$$

$$+ \left\| \frac{\alpha_f \beta_{s,0}}{\Delta t} \left(\widetilde{\gamma}_s \widetilde{\boldsymbol{\eta}}_s^{k+1} - \widetilde{\gamma}_s \widetilde{\boldsymbol{\eta}}_s^k\right) + \widetilde{\boldsymbol{\lambda}}_s^{k+1} - \widetilde{\boldsymbol{\lambda}}_s^k \right\|_Z + \|\mathcal{G}_s - \mathcal{S}(\widetilde{\boldsymbol{\eta}}_s^{k+1}) - \widetilde{\gamma}_s^* \widetilde{\boldsymbol{\lambda}}_s^{k+1}\|_K$$

$$\leq \varepsilon_1 + \varepsilon_2 \min \left\{ \|\widetilde{\boldsymbol{\eta}}_s^{k+1}\|_X; \|(\boldsymbol{u}_f^{k+1} \cdot \nabla)\boldsymbol{u}_f^{k+1}\|_W; \|\mathcal{G}_s - \mathcal{S}(\widetilde{\boldsymbol{\eta}}_s^0) - \widetilde{\gamma}_s^* \widetilde{\boldsymbol{\lambda}}_s^0\|_K; \left\| \frac{\alpha_f \beta_{s,0}}{\Delta t} \widetilde{\gamma}_s \widetilde{\boldsymbol{\eta}}_s^{k+1} + \widetilde{\boldsymbol{\lambda}}_s^{k+1} \right\|_Z \right\}.$$

Here X, W, Z, K are suitable Sobolev spaces. In particular, the right choice should be $X = H^{1/2}(\Sigma^0)$, $W = H^{-1}(\Omega_f)$, $Z = H^{-1/2}(\Sigma^0)$, $K = H^{-1}(\Omega_s)$.

However, due to the complexity in the computation of these norms, in practical implementations we consider $W = L^2(\Omega_f)$, $K = L^2(\Omega_s)$ and $Z = L^2(\Sigma^0)$.

This scheme is the most classical for haemodynamic applications (see, e.g., [12]), although we present it here with Robin-Robin interface conditions instead of the more common Dirichlet-Neumann choice. However, the use of just one loop for the treatment of both geometrical/physical non-linearities and interface continuity conditions, does not guarantee *a priori* a fast convergence towards the exact solution.

3.2 Double-loop scheme

We consider the following *two blocks Gauss-Seidel* preconditioner

$$\widehat{J}_{DL} = \left[\begin{array}{cc|cc} \mathcal{H} & \widetilde{\gamma}_m^* & & \\ \widetilde{\gamma}_m & & & \\ \hline & \widehat{\nabla}_{v_f}\mathcal{F} & \widetilde{\gamma}_f^* & \\ & \alpha_f\widetilde{\gamma}_f & I & I \quad -\alpha_f\frac{\beta_{s,0}}{\Delta t}\widetilde{\gamma}_s \\ \hline & -\alpha_s\widetilde{\gamma}_f & I & I \quad \alpha_s\frac{\beta_{s,0}}{\Delta t}\widetilde{\gamma}_s \\ & & & \widetilde{\gamma}_s^* \quad \nabla_{\eta_s}\mathcal{S} \end{array}\right],$$

which corresponds to the sequential solution of the harmonic extension and of a linearized FSI problem. For the solution of the latter, since we are interested in partitioned algorithms, we use the following preconditioner (see [5])

$$\widehat{P}_{RR} = \left[\begin{array}{cc|cc} \widehat{\nabla}_{v_f}\mathcal{F} & \widetilde{\gamma}_f^* & & \\ \alpha_f\widetilde{\gamma}_f & I & & \\ \hline -\alpha_s\widetilde{\gamma}_f & I & I & \alpha_s\frac{\beta_{s,0}}{\Delta t}\widetilde{\gamma}_s \\ & & \widetilde{\gamma}_s^* & \nabla_{\eta_s}\mathcal{S} \end{array}\right].$$

This corresponds to considering two nested loops, an external one for the treatment of the interface position and of the physical (fluid and structure) non-linearities, and an internal one for the treatment of the interface continuity conditions through the RR scheme. In particular, we have the following algorithm:

Given the solution at iteration k, solve at the current iteration $k+1$ until convergence

1. The harmonic extension

$$\begin{cases} \mathcal{H}\,\widetilde{\boldsymbol{\eta}}_m^{k+1} + \widetilde{\gamma}_m^*\widetilde{\boldsymbol{\lambda}}_m^{k+1} = 0 & \text{in } \left([V_m]^3\right)^*, \\ \widetilde{\gamma}_m\widetilde{\boldsymbol{\eta}}_m^{k+1} = \widetilde{\gamma}_s\widetilde{\boldsymbol{\eta}}_s^k & \text{on } \Sigma^0, \end{cases}$$

   obtaining the new fluid domain and fluid domain velocity.

2. The linearized FSI problem. For its solution, we consider the following partitioned algorithm:
Given the solution at subiteration $l-1$, solve at the current subiteration l until convergence

   (a) The fluid subproblem with a Robin condition at the FS interface

$$\begin{cases} \widehat{\nabla}_{v_f}\mathcal{F}(\boldsymbol{u}_{f,l}^k - \boldsymbol{u}_m^{k+1})\,\boldsymbol{v}_{f,l}^{k+1} + \widetilde{\gamma}_f^*\widetilde{\boldsymbol{\lambda}}_{f,l}^{k+1} = \mathcal{G}_f & \text{in } \left([V_f^{k+1}]^3 \times Q^{k+1}\right)^*, \\ \alpha_f\gamma_f\boldsymbol{v}_{f,l}^{k+1} + \boldsymbol{\lambda}_{f,l}^{k+1} = \alpha_f\gamma_s\left(\frac{\beta_{s,0}}{\Delta t}\boldsymbol{\eta}_{s,l-1}^k - \boldsymbol{f}_{s,U}\right) - \boldsymbol{\lambda}_{s,l-1}^k & \text{on } \Sigma^{k+1}, \end{cases}$$

   (b) The structure subproblem with a Robin condition at the FS interface

$$\begin{cases} \nabla_\eta\mathcal{S}(\widetilde{\boldsymbol{\eta}}_{s,l}^k)\,\delta\widetilde{\boldsymbol{\eta}}_{s,l}^{k+1} + \widetilde{\gamma}_s^*\delta\widetilde{\boldsymbol{\lambda}}_{s,l}^{k+1} = \mathcal{G}_s - \mathcal{S}(\widetilde{\boldsymbol{\eta}}_s^k) - \widetilde{\gamma}_s^*\widetilde{\boldsymbol{\lambda}}_s^k & \text{in } \left([V_s]^3\right)^*, \\ \alpha_s\dfrac{\beta_{s,0}}{\Delta t}\,\widetilde{\gamma}_s\,\widetilde{\boldsymbol{\eta}}_{s,l}^{k+1} - \widetilde{\boldsymbol{\lambda}}_{s,l}^{k+1} = \alpha_s\widetilde{\gamma}_f\,\widetilde{\boldsymbol{v}}_{f,l}^{k+1} - \widetilde{\boldsymbol{\lambda}}_{f,l}^{k+1} + \alpha_s\widetilde{\gamma}_s\widetilde{\boldsymbol{f}}_{s,U} & \text{on } \Sigma^0. \end{cases}$$

From (11), we obtain the following stopping criterion for the external loop

$$\begin{aligned} &\|\widetilde{\gamma}_s\,\widetilde{\boldsymbol{\eta}}_s^{k+1} - \widetilde{\gamma}_s\,\widetilde{\boldsymbol{\eta}}_s^k\|_X + \|((\boldsymbol{u}_f^{k+1} - \boldsymbol{u}_f^k)\cdot\nabla)\,\boldsymbol{u}_f^{k+1}\|_W + \|\mathcal{G}_s - \mathcal{S}(\widetilde{\boldsymbol{\eta}}_s^{k+1}) - \widetilde{\gamma}_s^*\widetilde{\boldsymbol{\lambda}}_s^{k+1}\|_K \quad (14) \\ &\leq \varepsilon_1 + \varepsilon_2 \min\left\{\|\widetilde{\boldsymbol{\eta}}_s^{k+1}\|_X; \|(\boldsymbol{u}_f^{k+1}\cdot\nabla)\boldsymbol{u}_f^{k+1}\|_W; \|\mathcal{G}_s - \mathcal{S}(\widetilde{\boldsymbol{\eta}}_s^0) - \widetilde{\gamma}_s^*\widetilde{\boldsymbol{\lambda}}_s^0\|_K\right\}, \end{aligned}$$

while for the internal loop we have (see [5])

$$\left\|\frac{\alpha_f\beta_{s,0}}{\Delta t}\left(\widetilde{\gamma}_s\widetilde{\boldsymbol{\eta}}_{s,l}^{k+1} - \widetilde{\gamma}_s\,\widetilde{\boldsymbol{\eta}}_{s,l-1}^{k+1}\right) + \widetilde{\boldsymbol{\lambda}}_{s,l}^{k+1} - \widetilde{\boldsymbol{\lambda}}_{s,l-1}^{k+1}\right\|_Z \leq \varepsilon_3 + \varepsilon_4\left\|\frac{\alpha_f\beta_{s,0}}{\Delta t}\widetilde{\gamma}_s\widetilde{\boldsymbol{\eta}}_{s,l}^{k+1} + \widetilde{\boldsymbol{\lambda}}_{s,l}^{k+1}\right\|_Z. \quad (15)$$

The use of two different loops for the geometrical/physical non-linearities and for the imposition of the interface continuity conditions makes this scheme more robust compared to the *Single-loop* scheme.

3.3 Hybrid schemes

Single loop scheme can be regarded as a Double loop scheme where just one internal iteration is performed. However, in the stopping criterion of the "external loop" the satisfaction of the interface continuity conditions is also monitored, so that this scheme is completely implicit and then exact. It is therefore reasonable to ask whether by performing (at most) $n > 1$ internal iterations, with n fixed, the CPU time decreases with respect to Double loop and Single loop schemes. For this reason, we propose here new hybrid schemes, obtained by performing at most n internal iterations in the Double Loop scheme. The criterion on the satisfaction of the interface continuity conditions is however checked in the external loop, so that these schemes are in fact completely implicit and exact (*hybrid schemes-n, HS-n*).

3.4 Inexact schemes

In order to improve the performances of the proposed algorithms in terms of CPU time, we propose here another family of algorithms drawn from the *Double-loop* scheme. We restrict here to the case of the linear infinitesimal elasticity only. The starting point is the observation that semi-implicit schemes [13, 9, 10, 11, 16] can be regarded as a Double loop scheme where the number of external iterations is fixed and equal to 1. For such schemes, the stopping criterion on the geometrical and physical non-linearities is not checked, so that they are in principle inexact. However, as observed in the Introduction, these schemes have been seen to be stable and accurate for the linearized infinitesimal elasticity, although no results are known for the non-linear finite elasticity. Now, it reasonable to ask whether the accuracy of semi-implicit schemes could be improved by performing at most $m > 1$ iterations in the external loop, where m is fixed. Again, in general these schemes are inexact, since we do not solve exactly the geometrical and fluid non-linearities. We refer to them as *geometrical and convective inexact schemes-m* (GCIS-m). We observe that in GCIS-1 just one external iteration is performed, so that this in fact is a semi-implicit scheme. Then, GCIS-m schemes, with $m > 1$, can be regarded as intermediate cases between semi-implicit and implicit algorithms. Our numerical results show that these schemes are very promising and perform well for the linear infinitesimal case. We are currently working on extending them to the non-linear case.

For what concerns the stopping criterion, one has to check just the satisfaction of (15).

3.5 Extrapolation from previous time steps

We are also interested in studying how the accuracy of inexact schemes and/or the efficiency (in terms of number of (external) iterations) of exact schemes could be possibly improved when considering at each new time step suitable extrapolations of order q of the interface quantities, structure displacement and fluid convective term, from previous time steps, q being the order of the temporal schemes. To this aim, we refer to the schemes with extrapolation as *Double-loop-extrap*, *Single-loop-extrap*, *HS-n-extrap* and *GCIS-m-extrap*. We anticipate here that no improvements are noticed in the numerical experiments by using GCIS-m-extrap with respect to GCIS-m, with $m \geq 2$. For this reason, among the GCIS-m-extrap schemes we consider just GCIS-1-extrap. In particular, this scheme is obtained by performing just one external iteration as for GCIS-1, but using as fluid domain quantities and convective term, extrapolations of order q from previous time steps. Obviously, GCIS-1 and GCIS-1-extrap do coincide for first order approximations.

For BDF schemes the extrapolation of order q is obtained by setting at the first external iteration ($k = 0$) $\boldsymbol{z}^{n+1,0} = \sum_{i=0}^{p} i\beta_i \boldsymbol{z}^{n+1-i}$, where $\boldsymbol{z}$ is one of the extrapolated variables, namely the structural displacement, the fluid velocity,

the fluid mesh velocity and the interface displacement. For the Newmark/theta-methods, since it is at most second order accurate, we use the following extrapolation $\boldsymbol{z}^{n+1,0} = \boldsymbol{z}^n + \Delta t \boldsymbol{d}^n$, where $\boldsymbol{d}$ is the discrete approximation of the time derivative of $\boldsymbol{z}$.

4 Numerical results

4.1 Generalities

In the numerical simulations considered in this work, we consider either the linear equations of infinitesimal elasticity with a constitutive law characterized by the following Piola-Kirchhoff stress tensor

$$\widetilde{\boldsymbol{T}}_s(\widetilde{\boldsymbol{\eta}}_s) = \frac{E\nu}{(1+\nu)(1-2\nu)} \operatorname{tr}(\boldsymbol{\epsilon}(\widetilde{\boldsymbol{\eta}}_s))\, \boldsymbol{I} + \frac{E}{2(1+\nu)} \boldsymbol{\epsilon}(\widetilde{\boldsymbol{\eta}}_s), \tag{16}$$

where $\boldsymbol{\epsilon}(\boldsymbol{\eta}) := \frac{(\nabla\boldsymbol{\eta} + (\nabla\boldsymbol{\eta})^T)}{2}$, E is the Young modulus, and ν is the Poisson ratio, or the non-linear equations of finite elasticity characterized by the Piola-Kirchhoff stress tensor of a St. Venant-Kirchhoff material, given by [32]

$$\widetilde{\boldsymbol{T}}_s(\widetilde{\boldsymbol{\eta}}_s) = \frac{E\nu}{(1+\nu)(1-2\nu)} \left(tr(\boldsymbol{F}_s^T \boldsymbol{F}_s) - 3\right) \boldsymbol{F}_s - \frac{E}{2(1+\nu)} \boldsymbol{F}_s + \frac{E}{2(1+\nu)} \boldsymbol{F}_s \boldsymbol{F}_s^T \boldsymbol{F}_s. \tag{17}$$

We consider the FSI problem (1), with $\mathcal{D} = 0$. Moreover, we used $P1bubble - P1$ finite elements for the fluid subproblem and $P1$ finite elements for the structure subproblem, and the following data: viscosity $\mu = 0.03\, dyne/cm^2$, fluid density $\rho_f = 1\, g/cm^3$, structure density $\rho_s = 1.2\, g/cm^3$, Young modulus $E = 3 \cdot 10^6\, dyne/cm^2$, Poisson ratio $\nu = 0.45$, time discretization parameter $\Delta t = 0.001\, s$.

For the prescription of the interface continuity conditions, in all the simulations we have considered the RR scheme, with the optimized coefficients proposed in [31]. In particular, the optimization procedure adapted to the various temporal schemes leads to

$$\alpha_f = \frac{1}{\beta_{s,0}} \left(\frac{\xi_{s,0} \rho_s H_s}{\Delta t} + \tau \Delta t \right),$$

where $\tau := \frac{E H_s \sqrt{\pi}}{(1-\nu^2) R^2}$, with R a reference radius, and

$$\alpha_s = \frac{2}{\Delta t\, k^*} \sqrt{\rho_f + \mu \Delta t\, (k^*)^2} \left(\sqrt{\mu \Delta t}\, k^* + \sqrt{\rho_f + \mu \Delta t\, (k^*)^2} \right),$$

with $k^* = \sqrt{\frac{\beta_{f,0} \rho_f (\sqrt{5}-1)}{2\mu \Delta t}}$. In all the simulations of this work, RR scheme has converged without any relaxation, confirming its suitability for haemodynamics applications.

The results have been obtained with the parallel Finite Element library `LIFEV` developed at MOX - Politecnico di Milano, INRIA - Paris, CMCS - EPF of Lausanne and Emory University - Atlanta. The management of the parallelism relies on `ParMETIS` (http://glaros.dtc.umn.edu/
gkhome/views/metis), whilst the solution of the linear system on `Trilinos` (http://trilinos.sandia.gov). In particular, the fluid and structure linear systems are solved with GMRes, whilst the harmonic extension with Coniugate Gradient, all preconditioned with an Additive Schwartz preconditioner available in the package `Ifpack` of Trilinos. The simulations were run on a cluster at the consortium `CILEA` (www.cilea.it, Segrate, Milan, Italy), with a 2-ways nodes Intel Xeon3.16 Ghz QuadCore as CPU and 16GB of ram per node.

4.2 Definition of the temporal schemes

Here, we introduce the temporal schemes we have considered in the numerical simulations. For what concerns the BDF schemes, in Table 1 we collect the values of the parameters β_i and ξ_i characterizing the method with order $q = 1, 2, 3, 4$. In what follows, we refer to the BDF scheme of order q as *BDFq*.

Regarding the Newmark/theta-methods, in Table 2 we report the values of the coefficients involved in the discretization, as a function of parameter θ for first order derivatives and of parameters θ and a for second order derivatives. These parameters completely describe the method. In particular, for the fluid momentum equation, we obtain the theta-method with parameter θ. In this work we consider the *Midpoint* scheme, that is $\theta = 2$ and $a = 0.25$, for the structure, and *Crank-Nicolson*, that is $\theta = 0.5$, for the fluid.

4.3 Boundary conditions

In all the simulations of this section, for the harmonic extension and for the structure, we prescribe at the artificial sections normal homogeneous Dirichlet conditions and tangential homogeneous Neumann conditions, that is we let the domain move freely in the tangential direction. Moreover, at the fluid inlet we prescribe a specific flow rate (detailed case by case) through the Lagrange multipliers method (see [33, 34]). At the outlet, we propose to use an absorbing boundary condition, obtained by following [11]. However, differently from [11], here we want to focus on a condition which relates implicitly the flow rate and the mean pressure. By introducing the characteristic variables W_1 and W_2 related to a reduced one-dimensional FSI problem [35] and by setting $W_2|_\Gamma = 0$, we obtain an absorbing boundary condition at the outlet Γ, which corresponds to

$$Q = g(P) = 4\gamma^* A(P) \left(A(P)^{1/4} - A_0^{1/4} \right) \quad \text{on } \Gamma, \tag{18}$$

where Q is the flow rate, A is the area related to the mean pressure P through the *algebraic law*

$$A = \left(\frac{(P - P_{ext})\sqrt{\pi}}{\tau(A)} + A_0^{1/2} \right)^2, \tag{19}$$

$\gamma = \sqrt{\frac{\tau(A)}{2\rho_f\sqrt{\pi}}}$, with P_{ext} the external pressure. We observe that the algebraic law (19) gives an implicit expression for the area A, since τ depends on A itself. For this reason, we set $\tau^* = \tau(A^*)$ and $\gamma^* = \gamma(A^*)$, where A^* is a reference value, which eventually could be updated during iterations. It is known that the choice of avoiding any reflection is not physiological, since some of them could occur from the peripheral system. However, in absence of data concerning the downstream cardiovascular tree, the choice of imposing absorbing boundary conditions seems to be acceptable. By considering the following Taylor expansion of (18) around a reference value $\widehat{P}$

$$Q = g(\widehat{P}) + \left.\frac{\partial g}{\partial P}\right|_{P=\widehat{P}} (P - \widehat{P}) \quad \text{on } \Gamma,$$

and approximating the mean pressure with the mean normal stress, we obtain the following *defective resistance boundary condition* in the normal direction [36]

$$\frac{1}{|\Gamma|}\int_\Gamma (\boldsymbol{T}_f\,\boldsymbol{n})\cdot\boldsymbol{n}\,d\sigma - \widehat{R}\int_\Gamma \boldsymbol{u}\cdot\boldsymbol{n}\,d\sigma = \widehat{P} - \widehat{R}\,g(\widehat{P}) \quad \text{on } \Gamma,$$

where $\widehat{R} := \left(\left.\frac{\partial g}{\partial P}\right|_{P=\widehat{P}}\right)^{-1}$ is the *resistance*, corresponding to

$$\widehat{R} = \sqrt{\frac{\rho_f\tau^*}{2\sqrt{\pi}}}\left.\left(\frac{1}{5A(\widehat{P})^{3/4} - 4A_0^{1/4}A(\widehat{P})^{1/2}}\right)\right|_\Gamma.$$

A first very simple choice consists in choosing $\widehat{P} = P_{ext}$ at each time step, leading to

$$\frac{1}{|\Gamma|}\int_\Gamma (\boldsymbol{T}_f\,\boldsymbol{n})\cdot\boldsymbol{n}\,d\sigma - R_e\int_{\Gamma^n} \boldsymbol{u}\cdot\boldsymbol{n}\,d\sigma = P_{ext} \quad \text{on } \Gamma, \tag{20}$$

where $R_e = \sqrt{\frac{\rho_f\tau^0}{2\sqrt{\pi}}}\,\frac{1}{A_0^{3/4}}$, $\tau^0 = \tau(A_0)$. Notice that $g(P_{ext}) = 0$.

In the simulations presented in Sections 4.4.1 and 4.4.3, we consider condition (20) at the outlets, with $P_{ext} = 0\,mmHg$.

4.4 Comparison among different schemes

In this section, we show the numerical results concerning the performance of the different algorithms proposed in Section 3.

4.4.1 Cylindrical domain - linear infinitesimal elasticity

We consider here the linear elastic behavior characterized by (16) and the cylindrical geometry depicted in Figure 2, where the length is $L = 5\,cm$, the fluid domain radius $R = 0.5\,cm$, the structure thickness $H_s = 0.1\,cm$, and the elastic coefficient of the surrounding tissue $\alpha_e = 3 \cdot 10^6\,dyne/cm^3$. This value has been extracted by the experimental results reported in [26] and allows to recover a pressure in the physiological range. We observe that this choice corresponds to

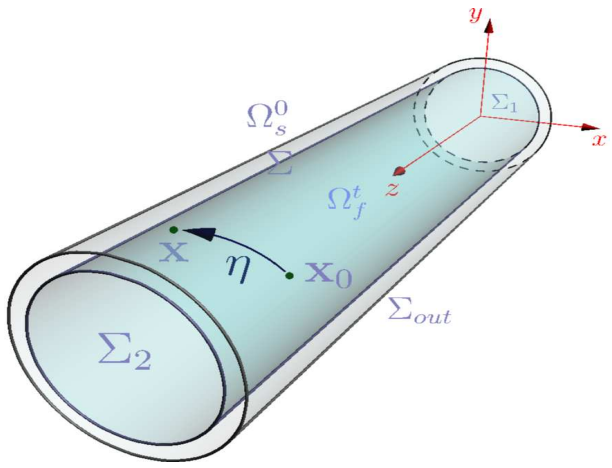

Figure 2: Cylindrical geometry.

a Young modulus of the surrounding tissue equal to $\alpha_e\, H_{ST}$, where H_{ST} is the thickness of the surrounding tissue. We prescribe the following flow rate Q_{in} at the inlet

$$Q_{in} = \begin{cases} 30\,\sin\left(25\pi t\right), & t \leq 0.04\,s, \\ 0 & 0.04\,s < t \leq T, \end{cases}$$

where $T = 0.08\,s$. The space discretization parameter is $h = 0.025\,cm$ and the fluid and structure meshes are conforming at the interface. We have about 15000 d.o.f. for the fluid and about 9000 for the structure. The tolerances used in criteria (13), (14) and (15) are $\varepsilon_1 = \varepsilon_2 = 10^{-8}$ and $\varepsilon_3 = \varepsilon_4 = 10^{-9}$. We ran all the simulations on 3 processors for the solution of the fluid problem and on 1 processor for the structure.

In the first set of simulations, we consider a global first order scheme, namely BDF1 for the fluid (that is *backward Euler*) and BDF1 for the structure (BDF1/BDF1). We remind that in this case GCIS-1 and GCIS-1-extrap schemes coincide. In Figure 3, we report a comparison of mean quantities of the solution at a section Σ located at $2.5\,cm$ from the inlet, obtained with Double-loop, GCIS-1, GCIS-2. We do not report the trends obtained by the other implicit schemes (Single-Loop and HS-n), since they are exact, so that the solution coincides with that of the Double-loop scheme. These results show that there is a general agree-

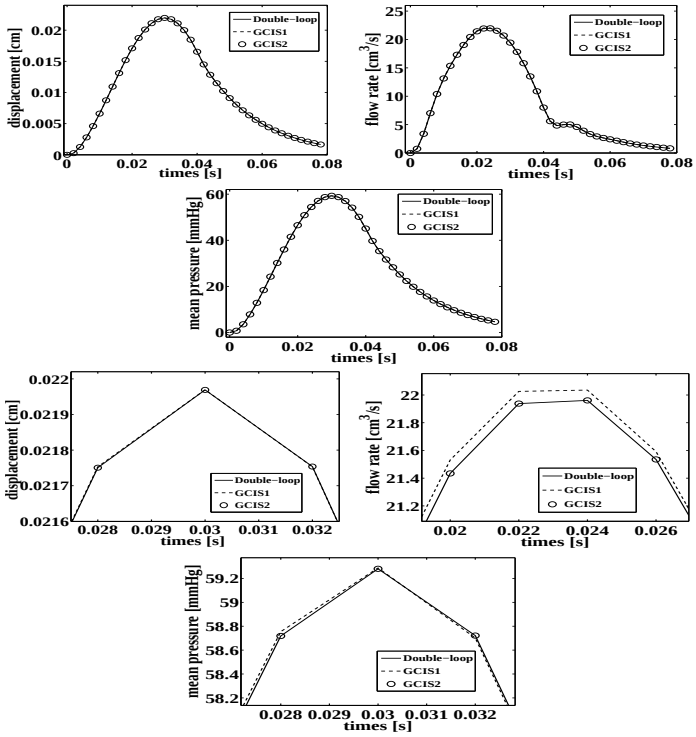

Figure 3: The comparison of the solution obtained with different schemes is reported at a section Σ located at $2.5\,cm$ from the inlet (up: whole interval, bottom: a zoom around the peak instant). Displacement of a point at the FS interface (left), flow rate (middle), mean pressure (right) - BDF1-BDF1.

ment among all the solutions. By taking the solution obtained with Double-loop scheme as the reference one, and zooming the solutions around the peak instant, it is possible to see that GCIS-1 features slight errors for the displacement and the mean pressure. In order to quantify these errors, we report the relative errors by using the solution obtained with Double-loop scheme as the reference one. In particular, in Tab. 3 we report the L^∞-norm at the peak instant of average quantities, namely the mean structure displacement η, the flow rate Q or the mean pressure P. To do this, we compute

$$\frac{\max_j |x^j_{DL} - x^j_*|}{\max_j |x^j_{DL}|} \tag{21}$$

at the peak instant, where x^j is one the average quantities computed at different sections Σ_j, DL stands for Double-loop and * stands for one of the other schemes. In Table 4, we show the relative errors at section Σ computed with

$$\frac{\|x_{DL} - x_*\|_{L^\infty(0,T)}}{\|x_{DL}\|_{L^\infty(0,T)}}, \tag{22}$$

where x is one of the average quantities at section Σ. From these results, we observe that Single-loop and HS-n schemes give, as expected, the same solution as Double-loop up to the tolerances chosen. Among the other schemes, GCIS-m schemes exhibit an excellent accuracy for $m = 1, 2, 3$, with an error in any case less than 0.5%. Moreover, we can observe that each external iteration reduces the error of about one order of magnitude. This shows that if convergence is reached in the internal (RR) loop, then it is not necessary to reach convergence also in the external loop, and just few (even one) external iterations are enough to obtain an accurate solution.

In Table 5 we report the mean number of iterations over the different time instants, in the external and in the internal loop (in the latter case they have to be intended as the averaged value per outer loop), and the CPU time normalized with respect to that of Double-loop scheme. From these results, we observe that Single-loop scheme is more expensive than Double-loop scheme. This could be explained by the fact that for the latter scheme the matrices are assembled only about 7 times per time step (since in the internal loop the matrices are not updated), against almost 14 times in Single-loop scheme. However, the results obtained by HS-n schemes, n=2,3, show that by performing just 2 or 3 internal iterations, the CPU time decreases. In particular, the computational effort decreases when n increases from 1 to 3. Again, this should be due to the fact the at each external loop we have to re-assemble the matrices. In particular HS-3 scheme improves efficiency of 28% with respect to Double-Loop scheme. Regarding GCIS-m schemes, we notice that they are very efficient, the CPU time being reduced up to 4 times with respect to Double-loop. This makes this family of schemes very appealing for applications, since they improve the CPU time with respect to classical schemes, without affecting considerably the accuracy.

In Tab. 6, we report the errors obtained by using the *Midpoint* scheme for the structure and the *Crank-Nicolson* scheme for the fluid, for GCIS-m schemes. These results confirm the trend highlighted by the results of the first order simulations. We also observe that GCIS-1-extrap is more accurate than GCIS-1. This is due to the second order extrapolations of the fluid domain quantities. The computation of CPU time of both exact and inexact schemes leads to the same conclusions as for BDF1/BDF1, and therefore we have not included them here.

Finally, we want to understand if, when considering high order methods for implicit schemes, a suitable extrapolation of the FS interface, fluid convective term and structure displacement could improve the efficiency, by providing a better starting point and decreasing consequently the number of external iterations. Observe that the solution does not change as we are acting only on the initial guess. In Table 7 we report the average number of iterations for implicit schemes with and without extrapolations from previous time steps. These results show that when considering extrapolations a slight improvement in the efficiency is observed for BDF2/BDF2, whilst no significant improvement is observed for

BDF3/BDF3, so we conclude that extrapolations are not necessary for implicit schemes.

In order to understand if the performance highlighted by the results of this section depends on the choice of the discretization parameters, we ran all the experiments also for $h = \widetilde{h}/2,\ 2\widetilde{h}$ and $\Delta t = \widetilde{\Delta t}/2,\ 2\widetilde{\Delta t}$, where $\widetilde{h}$ and $\widetilde{\Delta t}$ are the reference parameters. From these results we found that qualitatively the performance of the schemes is unchanged, so that we did not report these results in the text.

4.4.2 Cylindrical domain - non-linear finite elasticity

We consider here the non-linear elastic structure characterized by (17), and the same test and geometrical, physical and numerical parameters of the previous section. In this case we consider just implicit schemes, that is Double-loop, Single-loop, and HS-n schemes. Being these methods "exact", we do not report any accuracy results, but we limit our analysis just to efficiency. In particular, in Table 8 we show the mean number of iterations and the mean CPU time per time step featured by the methods. The results are very similar to the case of linear infinitesimal elasticity, and therefore we conclude that among the considered implicit algorithms, HS-3 scheme seems to be the most efficient even in the case of non-linear finite elasticity, reducing the CPU time of about 32% with respect to those of the Double loop scheme.

4.4.3 Carotid domain

In this section we show the numerical results obtained in a real geometry of a human carotid. We consider the linear infinitesimal elastic structure characterized by (16). The aim here is to compare three of the methods described in the previous section, namely Double-loop, CGIS-1 and GCIS-2, being the latter two the most promising in terms of CPU time. In particular, at the inlet we prescribe the physiological flow-rate depicted in Figure 4. Again we use as elastic

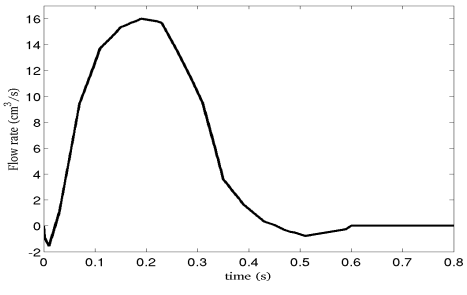

Figure 4: Flow rate waveform prescribed at the inlet of the carotid.

coefficient of the surrounding tissue $\alpha_e = 3 \cdot 10^6\, dyne/cm^3$. The tolerances used

in criteria (13), (14) and (15) are $\varepsilon_1 = \varepsilon_2 = 10^{-7}$ and $\varepsilon_3 = \varepsilon_4 = 10^{-8}$. We consider BDF1/BDF1 and ran the simulations on 15 processors for the solution of the fluid problem and on 1 processor for the structure.

In Figure 5, we show the wall shear stress at the peak instant (systole) computed with the three methods. We observe an excellent agreement among

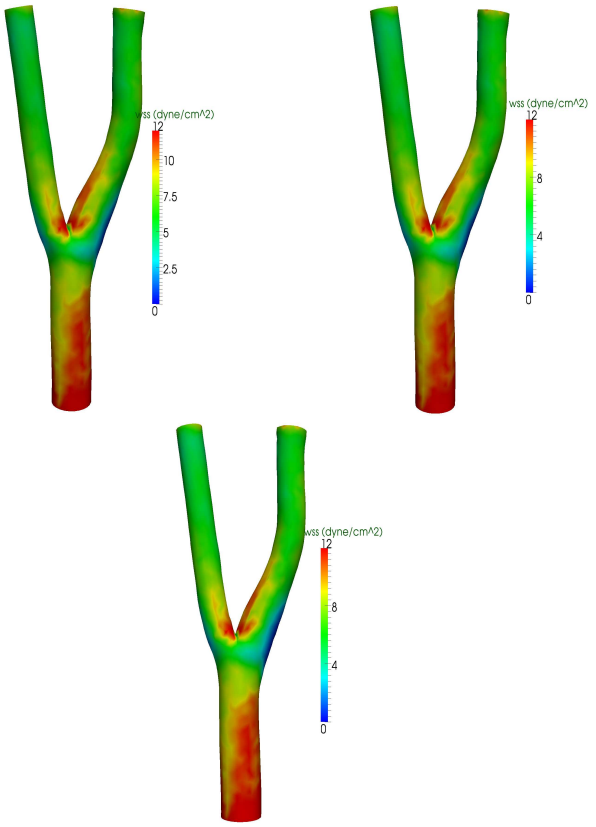

Figure 5: Wall shear stress at the systole computed with Double loop (left), GCIS-1 (middle) and GCIS-2 (right).

the three solutions. Moreover, the CPU time of GCIS-1 scheme normalized over that of Double loop is 0.30, whilst that of GCIS-2 is 0.47. These results confirm the accuracy and efficiency of GCIS-1 and GCIS-2 also for real applications, and therefore suggest that these methods could represent effective choices in the context of patient-specific simulations.

5 Convergence with respect to time

In this section, we aim at studying the time convergence order of the proposed inexact schemes. With this aim, in the next section we consider an analytical

test case, whilst in Section 5.2 we show some numerical results.

5.1 An analytical test case

In this section, we propose an analytical solution for the FSI problem in a 3D geometry, with the aim at validating the methods previously introduced, by the comparison between the exact and the numerical solutions.

We consider a straight cylinder as fluid domain and the extrusion of its lateral surface with a given thickness as structure domain. Referring to Figure 2, we consider the linear infinitesimal finite elasticity law (16) to describe the structure. We consider the FSI problem (1), with $\mathcal{D} = 0$ and with

$$\widetilde{\boldsymbol{\eta}}_s = \bar{\boldsymbol{\eta}} \quad \text{on } \Sigma^0_{out}, \tag{23}$$

instead of $(1)_6$, where

$$\bar{\boldsymbol{\eta}} := \begin{bmatrix} x^0_{s,1}(\cos\theta - 1) - x^0_{s,2}\sin\theta + c_1, \\ x^0_{s,1}\sin\theta + x^0_{s,2}(\cos\theta - 1) + c_2, \\ c_3, \end{bmatrix}$$

for given functions of time $\theta(t)$ and $\boldsymbol{c}(t)$. Moreover, we consider the following other boundary conditions

$$\begin{cases} \boldsymbol{u}_f = \bar{\boldsymbol{u}} & \text{on } \Sigma^t_{f,1} \cup \Sigma^t_{f,2}, \\ \widetilde{\boldsymbol{\eta}}_s = \bar{\boldsymbol{\eta}} & \text{on } \Sigma^0_{s,1} \cup \Sigma^0_{s,2}, \\ \widetilde{\boldsymbol{\eta}}_m = \bar{\boldsymbol{\eta}} & \text{on } \Sigma^0_{f,1} \cup \Sigma^0_{f,2}, \end{cases} \tag{24}$$

where

$$\bar{\boldsymbol{u}} := \begin{cases} \dot\theta(c_2 - x_{f,2}) + \dot c_1, \\ \dot\theta(x_{f,1} - c_1) + \dot c_2, \\ \dot c_3, \end{cases}$$

and the initial conditions

$$\begin{cases} \boldsymbol{u}_f = \bar{\boldsymbol{u}} & \text{for } t = 0, \\ \widetilde{\boldsymbol{\eta}}_s = \bar{\boldsymbol{\eta}} & \text{for } t = 0, \\ \frac{\partial \widetilde{\boldsymbol{\eta}}_s}{\partial t} = \frac{\partial \bar{\boldsymbol{\eta}}}{\partial t} & \text{for } t = 0. \end{cases} \tag{25}$$

Finally, we define the following forcing terms

$$\begin{aligned} \boldsymbol{f}_f &= \begin{cases} \rho_f \left(\dot\theta^2 (c_1 - x_{f,1}) + \ddot\theta (c_2 - x_{f,2}) + \ddot c_1 \right), \\ \rho_f \left(\dot\theta^2 (c_2 - x_{f,2}) + \ddot\theta (x_{f,1} - c_1) + \ddot c_2 \right), \\ \rho_f \ddot c_3, \end{cases} \\ \widetilde{\boldsymbol{f}}_s &= \begin{cases} -\rho_s \left(\ddot\theta \left(x^0_{s,1}\sin\theta + x^0_{s,2}\cos\theta \right) + \dot\theta^2 \left(x^0_{s,1}\cos\theta - x^0_{s,2}\sin\theta \right) - \ddot c_1 \right), \\ \rho_s \left(\ddot\theta \left(x^0_{s,1}\cos\theta - x^0_{s,2}\sin\theta \right) - \dot\theta^2 \left(x^0_{s,1}\sin\theta - x^0_{s,2}\cos\theta \right) - \ddot c_2 \right), \\ \rho_s \ddot c_3. \end{cases} \end{aligned} \tag{26}$$

It is easy to check that the analytical solution of $(1)_{1-5}$,(23), (24), (25) and (26) is given by

$$\begin{cases} \boldsymbol{u}_f = \bar{\boldsymbol{u}} & \text{in } \Omega_f^t, \\ p_f = \frac{E}{1+\nu}\left(1+\frac{2\nu}{1-2\nu}\right)(1-\cos(\theta)) & \text{in } \Omega_f^t, \\ \widetilde{\boldsymbol{\eta}}_s = \bar{\boldsymbol{\eta}} & \text{in } \Omega_s^0, \\ \widetilde{\boldsymbol{\eta}}_m = \bar{\boldsymbol{\eta}} & \text{in } \Omega_f^0. \end{cases}$$

This analytical solution represents a roto-translation of the points of the fluid-structure domain, that is $\boldsymbol{x}_i^t = R(t)\boldsymbol{x}_i^0 + \boldsymbol{c}(t)$, $i = f, s$, where

$$R(t) := \begin{bmatrix} \cos\theta & -\sin\theta & 0 \\ \sin\theta & \cos\theta & 0 \\ 0 & 0 & 1 \end{bmatrix}$$

represents the rotation, and $\boldsymbol{c}(t)$ is the vector representing the translation.

5.2 Numerical results

The geometrical properties of the domain are the same of Section 4.4.1, whilst $h = 0.015\,cm$. For what concerns the data of the test, we have set $\boldsymbol{c} = \boldsymbol{0}$ and $\theta(t) = 0.2(1 - cos(50\pi\, t))$. The tolerances used in criteria (13), (14) and (15) are $\varepsilon_1 = \varepsilon_2 = 10^{-7}$ and $\varepsilon_3 = \varepsilon_4 = 10^{-8}$ and we ran all the simulations on 31 processors for the solution of the fluid problem and on 1 processor for the structure.

In Figure 6 we show the convergence history of Double Loop, GCIS-1, GCIS-1-extrap and GCIS-2 schemes for three selected temporal schemes, namely BDF1/BDF1, BDF2/BDF2, Midpont/Crank-Nicolson, whilst in Figure 7 the convergence history of Double Loop, GCIS-1-extrap, GCIS-2 and GCIS-3 schemes for BDF3/BDF3 and BDF4/BDF4. We do not consider here Single Loop and HS-n schemes since they are exact, so that their behavior is the same of Double Loop scheme. A relative L^2 norm is computed at time $t = 0.002\,s$ for the first four schemes, whilst at $t = 0.001\,s$ for BDF4/BDF4. The time discretization parameter is $\Delta t = 2\cdot 10^{-3}$, 10^{-3}, $5\cdot 10^{-4}$, $2.5\cdot 10^{-4}\,s$ for the first four schemes, whilst we set $\Delta t = 10^{-3}$, $5\cdot 10^{-4}$, $3.3\cdot 10^{-4}$, $2.5\cdot 10^{-4}\,s$ for BDF4/BDF4. These results show that the expected convergence orders are achieved by the Double-loop scheme. We observe that for BDF4/BDF4, the behavior of the fluid velocity and structure displacement errors moves away from fourth order. This is probably due to the presence of the spatial error. GCIS-1 scheme is as expected first order accurate, whilst GCIS-1-extrap scheme allows to recover order q, showing that an extrapolation of order q of the FS interface and convective term is suitable to recover the right convergence order when performing just one external iteration. Moreover, when a m-th order discretization is considered, $m \geq 2$, GCIS-m schemes recover order m without any extrapolation. This is the reason why we have not considered GCIS-m-extrap schemes with $m \geq 2$ in this work. More interestingly, when a q-th order discretization is considered, GCIS-2 recover order q without any extrapolation even for $q = 3$ or $q = 4$.

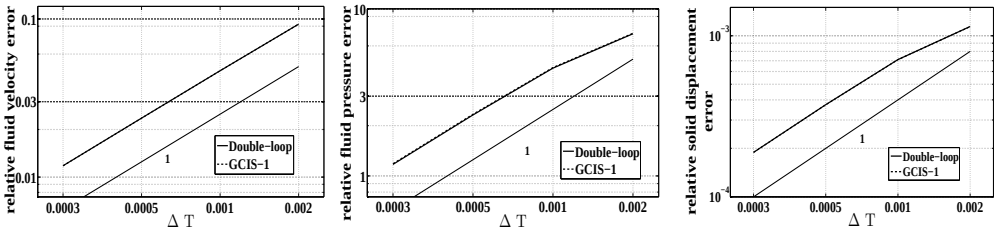

(a) BDF1/BDF1

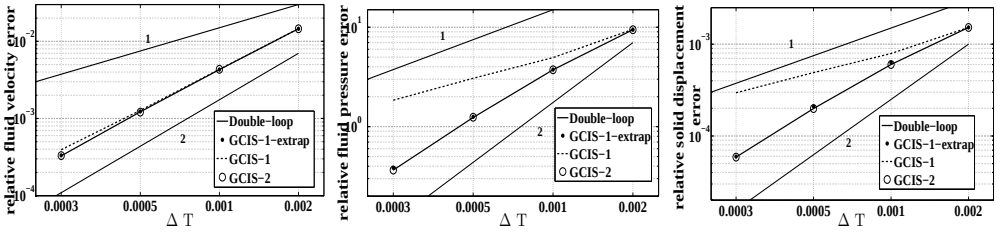

(b) BDF2/BDF2

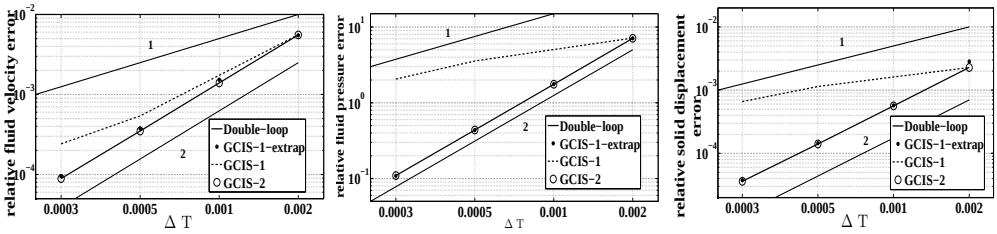

(c) Midpoint/Crank-Nicolson

Figure 6: Convergence rate of three temporal schemes considered. Relative errors of the fluid velocity (left), of the pressure (middle) and of the structure displacement (right) - BDF1/BDF1 (up), BDF2/BDF2 (middle), Midpoint/Crank-Nicolson (bottom) - $t = 0.002\,s$.

6 Conclusions

In this work we considered the numerical solution with partitioned schemes of the FSI problem in haemodynamics. We started from a suitable formulation of the monolithic system and we derived solution schemes as quasi-Newton preconditioners. Among them, we considered several approaches: implicit schemes, such as Double-Loop, Single-Loop and HS-n, and inexact schemes GCIS-m, as well as a purely geometry explicit scheme GCIS-1-extrap with a $q-th$ order ex-

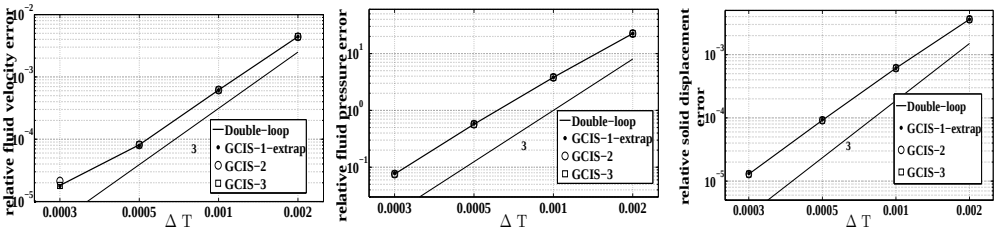

(a) BDF3/BDF3

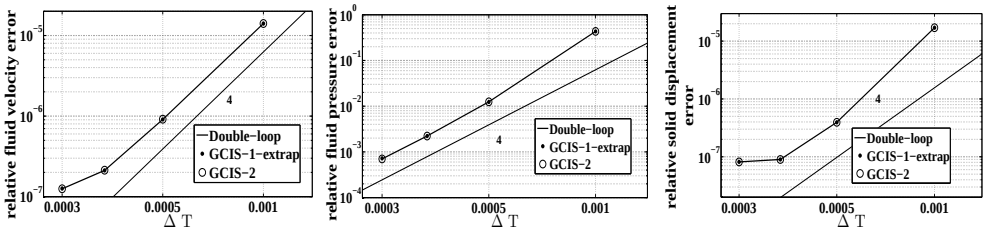

(b) BDF4/BDF4

Figure 7: Convergence rate of two temporal schemes considered. Relative errors of the fluid velocity (left), of the pressure (middle) and of the structure displacement (right) - BDF3/BDF3 - $t = 0.002\,s$ (up), BDF4/BDF4 - $t = 0.001\,s$ (bottom).

trapolation of the interface position as well as the fluid convective term. Implicit schemes were tested also in the case of non-linear finite elasticity. We summarize in what follows the conclusion we have drawn from the numerical solutions. In particular, for what concerns the efficiency of the schemes, we found that

1. Among implicit schemes, Single-loop is less efficient than Double-loop, and HS-3 scheme features the best efficiency (about 30% faster than Double-loop). These observations hold both in the case of linear infinitesimal and of non-linear finite elasticity;

2. An extrapolation of order q of geometrical quantities and of fluid convective term when using a $q-th$ order method does not improve the efficiency of implicit schemes;

3. in the case of linear infinitesimal elasticity, GCIS-m schemes, $m = 2, 3$, improve the efficiency with respect to Double-loop up to four and two times, respectively.

We also studied the accuracy with respect to time of the proposed schemes, by considering a new analytical test case for FSI problems in the case of linear

infinitesimal elasticity, and by applying temporal schemes of order q both for the fluid and for the structure subproblems. We found that

4. Implicit schemes, as expected, recover globally a q-th order scheme;

5. In the case of linear infinitesimal elasticity, GCIS-1 scheme needs a $q-th$ order extrapolation of interface geometrical quantities and of fluid convective term to recover globally a $q-th$ order scheme. Without any extrapolation it is as expected first order accurate;

6. In the case of linear infinitesimal elasticity, GCIS-m schemes, $m \geq 2$, do not need any extrapolation to recover a global order m. Moreover, we noticed that GCIS-2 recovers also order 3 and 4 when using BDF3/BDF3 or BDF4/BDF4, respectively, *without any extrapolation*.

In conclusion, we can state that among implicit schemes HS-3 seems to be preferable in terms of efficiency both in the case of linear infinitesimal and of non-linear finite elasticity, and that, among inexact schemes, GCIS-2 seems to be a very effective scheme in haemodynamics for the solution of FSI problems in the case of linear infinitesimal elasticity in real geometries.

References

[1] Perktold K, Thurner E, Kenner T. Flow and stress characteristics in rigid walled and compliant carotid artery bifurcation models. *Medical and Biological Engineering and Computing* 1994; **32**(1):19–26.

[2] Bazilevs Y, Calo V, Zhang Y, Hughes T. Isogeometric fluid-structure interaction analysis with applications to arterial blood flow. *Computational Mechanics* 2006; **38**:310–322.

[3] Figueroa C, Vignon-Clementel I, Jansen K, Hughes T, Taylor C. A coupled momentum method for modeling blood flow in three-dimensional deformable arteries. *Comput. Methods Appl. Mech. Engrg.* 2006; **195**:5685–5706.

[4] Tezduyar T, Sathe S, Cragin T, Nanna B, Conklin B, Pausewang J, Schwaab M. Modelling of fluid-structure interactions with the space-time finite elements: arterial fluid mechanics. *Int. J. Num. Methods Fluids* 2007; **54**:901–922.

[5] Badia S, Nobile F, Vergara C. Fluid-structure partitioned procedures based on Robin transmission conditions. *J. Comput. Physics* 2008; **227**:7027–7051.

[6] Formaggia L, Quarteroni A, (Eds) AV. *Cardiovascular Mathematics - Modeling and simulation of the circulatory system*. Springer, 2009.

[7] Heil M. An efficient solver for the fully coupled solution of large-displacement fluid-structure interaction problems. *Comput. Methods Appl. Mech. Engrg.* 2004; **193**:1–23.

[8] Fernández M, Moubachir M. A Newton method using exact Jacobians for solving fluid-structure coupling. *Computers & Structures* 2005; **83(2-3)**:127–142.

[9] Fernández M, Gerbeau J, Grandmont C. A projection semi-implicit scheme for the coupling of an elastic structure with an incompressible fluid. *Int. J. Num. Methods Engrg.* 2007; **69**(4):794–821.

[10] Badia S, Quaini A, Quarteroni A. Splitting methods based on algebraic factorization for fluid-structure interaction. *SIAM J Sc Comp* 2008; **30**(4):1778–1805.

[11] Nobile F, Vergara C. An effective fluid-structure interaction formulation for vascular dynamics by generalized Robin conditions. *SIAM J Sc Comp* 2008; **30**(2):731–763.

[12] Nobile F. Numerical approximation of fluid-structure interaction problems with application to haemodynamics. PhD Thesis, École Polytechnique Fédérale de Lausanne 2001. Thesis n° 2458.

[13] Swim E, Seshaiyer P. A nonconforming finite element method for fluid-structure interaction problems. *Comput. Methods Appl. Mech. Engrg.* 2006; (195):2088–2099.

[14] Murea CM, Sy S. A fast method for solving fluid-structure interaction problems numerically. *Int. J. Num. Methods Fluids* 2009; **60**:1149–1172.

[15] Astorino M, Grandmont C. Convergence analysis of a projection semi-implicit coupling scheme for fluid-structure interaction problems. *Numer Math* 2010; (116(4)):721–767.

[16] Crosetto P, Deparis S, Fourestey G, Quarteroni A. Parallel algorithms for fluid-structure interaction problems in haemodynamics. *EPFL-REPORT-148536* 2009; .

[17] Gee M, Kuttler U, Wall W. Truly monolithic algebraic multigrid for fluid-structure interaction. *Int. J. Num. Methods Engrg.* 2011; **85(8)**:987–1016.

[18] Barker A, Cai XC. Scalable parallel methods for monolithic coupling in fluid-structure interaction with application to blood flow modeling. *J. Comput. Phys.* 2010; **229**:642659.

[19] Piperno S, Farhat C. Design of efficient partitioned procedures for transient solution of aerolastic problems. *Rev. Eur. Elements Finis* 2000; **9(6-7)**:655–680.

[20] Causin P, Gerbeau J, Nobile F. Added-mass effect in the design of partitioned algorithms for fluid-structure problems. *Comput. Methods Appl. Mech. Engrg.* 2005; **194(42-44)**:4506–4527.

[21] Deparis S, Discacciati M, Fourestey G, Quarteroni A. Fluid-structure algorithms based on Steklov-Poincaré operators. *Comput. Methods Appl. Mech. Engrg.* 2006; **195**(41-43):5797–5812.

[22] Forster C, Wall W, Ramm E. Artificial added mass instabilities in sequential staggered coupling of nonlinear structures and incompressible viscous flow. *Comput. Methods Appl. Mech. Engrg.* 2007; **196**(7):1278–1293.

[23] Hughes TJR, Liu WK, Zimmermann TK. Lagrangian-Eulerian finite element formulation for incompressible viscous flows. *Comput. Methods Appl. Mech. Engrg.* 1981; **29**(3):329–349.

[24] Donea J. An arbitrary Lagrangian-Eulerian finite element method for transient dynamic fluid-structure interaction. *Comput. Methods Appl. Mech. Engrg.* 1982; **33**:689–723.

[25] Moireau P, Xiao N, Astorino M, Figueroa CA, Chapelle D, Taylor CA, Gerbeau JF. External tissue support and fluidstructure simulation in blood flows. *Biomechanics and Modeling in Mechanobiology* 2011; doi:DOI 10.1007/s10237-011-0289-z.

[26] Liu Y, Charles C, Gracia M, Gregersen H, Kassab GS. Surrounding tissues affect the passive mechanics of the vessel wall: theory and experiment. *Am J Physiol Heart Circ Physiol* 2007; **293**:H3290–H3300.

[27] Hairer E, Nørsett S, Wanner G. *Solving ordinary differential equations: Nonstiff problems*. Springer series in computational mathematics, Springer, 1993.

[28] Hairer E, Wanner G. *Solving Ordinary Differential Equations II: Stiff and Differential-Algebraic Problems*. Springer Series in Computational Mathematics, Springer, 2010.

[29] Badia S, Nobile F, Vergara C. Robin-Robin preconditioned Krylov methods for fluid-structure interaction problems. *Comput. Methods Appl. Mech. Engrg.* 2009; **198**(33-36):2768–2784.

[30] Astorino M, Chouly F, Fernández M. Robin based semi-implicit coupling in fluid-structure interaction: stability analysis and numerics. *SIAM J Sc Comp* 2009; (31(6)):4041–4065.

[31] Gerardo Giorda L, Nobile F, Vergara C. Analysis and optimization of robin-robin partitioned procedures in fluid-structure interaction problems. *SIAM J. Numer. Anal.* 2010; **48(6)**:2091–2116.

[32] Holzapfel G, Gasser T, Ogden R. A new constitutive framework for arterial wall mechanics and a comparative study of material models. *Journal of elasticity* 2000; **61**(1):1–48.

[33] Formaggia L, Gerbeau JF, Nobile F, Quarteroni A. Numerical treatment of defective boundary conditions for the Navier-Stokes equation. *SIAM J. Numer. Anal.* 2002; **40(1)**:376–401.

[34] Veneziani A, Vergara C. Flow rate defective boundary conditions in haemodinamics simulations. *Int. J. Num. Methods Fluids* 2005; **47**:803–816.

[35] Formaggia L, Gerbeau JF, Nobile F, Quarteroni A. On the coupling of 3D an 1D Navier-Stokes equations for flow problems in compliant vessels. *Comput. Methods Appl. Mech. Engrg.* 2001; **191(6-7)**:561–582.

[36] Vergara C. Nitsches method for defective boundary value problems in incompressibile fluid-dynamics. *J Sci Comp* 2011; **46(1)**:100–123.

Tables

	β_0	β_1	β_2	β_3	β_4	ξ_0	ξ_1	ξ_2	ξ_3	ξ_4	ξ_5
1	1	1	–	–	–	1	2	-1	–	–	–
2	3/2	2	-1/2	–	–	2	5	-4	1	–	–
3	11/6	3	-3/2	1/3	–	35/12	26/3	-19/2	14/3	-11/12	–
4	25/12	4	-3	4/3	-1/4	15/4	77/6	-107/6	13	-61/12	5/6

Table 1: Values of parameters β_i and ξ_i for BDFq schemes involved in the discretization of first (left) and second (right) derivatives - $q = 1, 2, 3, 4$.

$\beta_0 = \beta_1$	χ	κ	$\xi_0 = \xi_1 = \sigma$	ζ
θ	$\theta - 1$	$\frac{\theta}{2} - 1$	$\frac{1}{a}$	$\frac{1}{2a} - 1$

Table 2: Values of the parameters for Newmark/theta-methods involved in the discretization of first (left) and second (right) derivatives, .

	η (%)	Q (%)	P(%)
Single loop	0.0006	0.0004	0.0002
HS-2	0.0009	0.0008	0.0002
HS-3	0.0009	0.0007	0.0006
GCIS-1	0.0845	0.3563	0.2548
GCIS-2	0.0023	0.0220	0.0008
GCIS-3	0.0001	0.0004	0.0001

Table 3: Relative error with respect to Double-loop scheme, computed with (21). BDF1/BDF1. Left: displacement. Middle: flow rate. Right: mean pressure. Peak instant $t = 0.02\,s$. Linear infinitesimal elasticity.

	η (%)	Q (%)	P (%)
Single loop	0.0009	0.0026	0.0009
HS-2	0.0006	0.0003	0.0001
HS-3	0.0006	0.0002	0.0001
GCIS-1	0.1182	0.4607	0.2076
GCIS-2	0.0005	0.0014	0.0010
GCIS-3	0.0001	0.0005	0.0002

Table 4: Relative error with respect to Double-loop scheme, computed with (22), at section Σ. BDF1/BDF1. Linear infinitesimal elasticity.

	# of external iterations	# of internal iterations	Normalized CPU time
Double-loop	7.1	5.2	1.00
Single-loop	13.7	-	1.13
HS-2	9.0	1.7	0.78
HS-3	7.2	2.7	0.72
GCIS-1	1.0	14.3	0.23
GCIS-2	2.0	12.0	0.45
GCIS-3	3.0	9.7	0.60

Table 5: Average number of iterations in the external loop and average number of iterations per outer loop in the internal one (for Single-loop the only loop is indicated as external) and CPU time normalized with respect to that of Double-loop scheme. BDF1/BDF1. Linear infinitesimal elasticity.

	η (%)	Q (%)	P (%)
GCIS-1	0.0794	0.0617	0.0531
GCIS-1-extrap	0.0321	0.0254	0.0213
GCIS-2	0.0315	0.0171	0.0208
GCIS-3	0.0012	0.0051	0.0008

Table 6: Relative error of inexact schemes with respect to Double-loop scheme, computed with (21). Midpoint/Crank-Nicolson. Left: displacement. Middle: flow rate. Right: mean pressure. Peak instant $t = 0.02\,s$. Linear infinitesimal elasticity.

	BDF1/BDF1	BDF2/BDF2	BDF3/BDF3
Single-loop	13.7	16.7	14.7
Single-loop-extrap	-	14.6	14.6
Double loop	7.1	7.6	6.7
Double-loop-extrap	-	6.2	6.5
HS-2	9.0	8.6	8.5
HS-2-extrap	-	7.9	8.3
HS-3	7.2	8.6	6.9
HS-3-extrap	-	7.4	6.7

Table 7: Average number of iterations for implicit schemes (in the external loop for Double loop). Linear infinitesimal elasticity.

	# of external iterations	# of internal iterations	Normalized CPU time
Double-loop	7.0	5.5	1.00
Single-loop	14.6	-	1.08
HS-2	8.7	1.8	0.81
HS-3	6.9	2.4	0.68

Table 8: Average number of iterations in the external loop and average number of iterations per outer loop in the internal one (for Single-loop the only loop is indicated as external) and CPU time normalized with respect to that of Double-loop scheme. Implicit schemes. BDF1/BDF1. Non-linear finite elasticity.

Recent publications :

MATHEMATICS INSTITUTE OF COMPUTATIONAL SCIENCE AND ENGINEERING
Section of Mathematics
Ecole Polytechnique Fédérale
CH-1015 Lausanne

01.2012 A. ABDULLE, A. NONNENMACHER:
A posteriori error estimate in quantities of interest for the finite element heterogeneous multiscale method

02.2012 F. NOBILE, M. POZZOLI, C. VERGARA:
Time accurate partitioned algorithms for the solution of fluid-structure interaction problems in haemodynamics